Electrochimica Acta 507 (2024) 145113

Contents lists available at ScienceDirect

Electrochimica Acta

journal homepage: www.journals.elsevier.com/electrochimica-acta

Repurposing discarded porphyrin waste as electrocatalysts for the oxygen reduction reaction

Nicolò Giulini [a], Mohsin Muhyuddin [a], Sara Mattiello [a], Mauro Sassi [a], Carmelo Lo Vecchio [b], Vincenzo Baglio [b], Enrico Berretti [c], Alessandro Lavacchi [c], Enza Fazio [d], Luca Beverina [a], Carlo Santoro [a,*]

[a] Department of Materials Science, University of Milano-Bicocca, U5 building, Via Cozzi 55, 20125 Milan, Italy
[b] Institute for Advanced Energy Technologies "Nicola Giordano" CNR-ITAE, Via Salita S. Lucia sopra Contesse 5, 98126 Messina, Italy
[c] Istituto di Chimica Dei Composti OrganoMetallici (ICCOM), Consiglio Nazionale Delle Ricerche (CNR),Via Madonna Del Piano 10, 50019 Sesto Fiorentino, Italy
[d] Department of Mathematical and Computer Sciences, Physical Sciences and Earth Sciences, University of Messina, Viale Ferdinando Stagno D'Alcontres 31, Messina, 98166, Italy

ARTICLE INFO

Keywords:
Oxygen reduction reaction
Platinum group metals-free
Porphyrins
Waste upcycling
Electrocatalysis

ABSTRACT

The oxygen reduction reaction (ORR), presently known as the key bottleneck in the mass-scale implementation of fuel cells (FCs), typically relies on the exploitation of scarce and expensive platinum group metals (PGMs). Meanwhile, as a substitute for PGMs, transition metal-nitrogen carbons (TM-N_x-C) are proving to be reliable electrocatalysts (ECs) in which atomically dispersed TMs coordinated with nitrogen are integrated into the carbon matrix. Such TM-N_x coordination already exists in metal-porphyrins making them suitable precursors for TM-N_x-C. Adler-Longo method is the standard recipe for meso-tetraphenyl porphyrin realizes ca. 20 % yield whereas the residual polypyrromethenes, structurally resembling open porphyrin rings, are often wasted. Herein, the possibility of upcycling waste polypyrromethenes into efficient TM-N_x-C for ORR is demonstrated. A comprehensive structural and morphological characterization is provided, and the electrocatalytic activity towards ORR in an alkaline environment is discussed using Fe and Mn as TMs. The EC synthesized from pure porphyrin precursor at 600 °C (FeTPP_600) had the best performance recording 0.972 and 0.852 V vs RHE for E_{onset} and $E_{1/2}$. Mixing porphyrins with their synthetic waste (ratio of 1:4) and pyrolyzing it at 800 °C (FeTPP/Waste(1:4)_800) still exhibits appreciable kinetics with similar results (0.977 and 0.853 V vs RHE for E_{onset} and $E_{1/2}$).

1. Introduction

An efficient way to transform the chemical energy of hydrogen into electricity is through electrochemical devices named fuel cells (FCs). [1] In hydrogen fuel cells, hydrogen is oxidized at the anode, and oxygen is reduced at the cathode. These red-ox reactions generate a flow of electrons that is harvested to generate electricity. Low-temperature (low-T) FCs are more promising for portable and automotive applications due to the lower time and energy required for start-up and shutdown. [2] The low-T FC with the higher technology readiness level (TRL) is the proton exchange membrane (PEM) FC. PEM-FC relies on anode and cathode electrodes of a platinum-containing catalytic layer supported over carbon (Pt/C) as the electrocatalyst. [3,4] These electrocatalysts are necessary for considerably enhancing the anodic and cathodic performance, despite substantially increasing the overall cost and hindering the widespread application of this technology. [5] From the technical point of view, the oxygen reduction reaction (ORR) is the limiting reaction and requires a large loading of platinum to overcome the large overpotentials and improve kinetics. [6–8] Indeed, one of the main focuses of research related to FCs is nowadays centered on ORR to enhance the electrocatalytic activity while reducing the quantity of platinum used and in the future, if possible, totally replacing it. [5,6,9–11]

Interestingly, in the past years, due to the development of anion exchange membranes (AEMs), great attention has been captured by fuel cells operating in an alkaline environment, the so-called AEM-FC. [12–16] The ORR in alkaline media can occur (i) through a direct 4e$^-$ transfer mechanism on a single active site forming hydroxides OH^-, (ii)

* Corresponding author.
E-mail address: carlo.santoro@unimib.it (C. Santoro).

https://doi.org/10.1016/j.electacta.2024.145113
Received 22 July 2024; Received in revised form 10 September 2024; Accepted 21 September 2024
Available online 22 September 2024

through a direct 2e$^-$ transfer mechanism on a single site forming OOH^-, or (iii) through a more complex 2 × 2e$^-$ transfer mechanism where O_2 is transformed into intermediates first (OOH^-) and then into the final product (OH^-). The last reaction can occur over the same active site with the desorption of the intermediate of two different active sites. [17–19]

The operation in an alkaline environment allows substituting Pt/C ORR electrocatalysts with platinum group metal-free (PGM-free) materials based on earth-abundant transition metals (TMs) including Fe, Co, Ni, Mn, Cu, etc. [20–23] It has been shown that atomically dispersed TMs coordinated with nitrogen in the following form TM-N_x ($x = 2,3,4$) integrated into a conductive carbon backbone are extremely active towards the ORR in alkaline environment [24,25] and in certain cases, they outperform Pt/C. [26] Particularly, Fe-N_x-C can outperform the other TM-based electrocatalysts. [27–29] Moreover, atomically dispersed Fe-N_x are the desired active sites responsible for the direct 4e$^-$ or the 2 × 2e$^-$ transfer mechanism. TMs in other forms such as metallic nanoparticles, oxides, carbides, etc. are not desired since they lead to an undesired 2e$^-$ transfer mechanism. [30]

In the literature, different synthetic routes are reported for fabricating Fe-N_x-C electrocatalysts. [31] The easiest, least sophisticated, least expensive, and easily scalable synthetic route to develop Fe-based ORR electrocatalysts consists of integrating aza-macrocyclic precursors containing the metal of interest into a carbon matrix. [32,33] These organic precursors can be purchased if they are available commercially or they can be synthesized from scratch. Afterward, the aza-macrocyclic complexes are mixed with a high surface area, electrically conductive, carbonaceous matrix, and then the mixture is subjected to controlled pyrolysis to chemically embed them into the carbon support. Several examples following this synthetic route are presented in literature exploiting as precursors porphyrins, phthalocyanines, corroles, tetraaza [14] annulenes, etc. with successful ORR electrocatalytic activity and stability. [34–46,42,47,48] Particularly, the evolution during controlled pyrolysis of the active sites of Fe-phthalocyanine supported over high surface area carbon was recently studied. [49]

Further approaches for fabricating electrocatalysts are based on metal-containing covalent organic frameworks (COFs) or metal-organic frameworks (MOFs). [50–54] COFs and MOFs are porous, three-dimensional, and crystalline networks that contain the metal of interest in their structure, bonded through organic linkers. Generally, after their synthesis, for electrochemical purposes, they are subject to pyrolysis to carbonize the structure and enhance the electrical conductivity of the materials while maintaining a highly porous three-dimensional structure. COFs and MOFs have shown very high electrocatalytic activity towards ORR with low intermediate formed and almost complete conversion following a direct 4e$^-$ transfer mechanism. [55–57] Among these ORR materials, interesting results were obtained from synthesizing high surface area aerogel that possesses high active site density (SD), high turnover frequency number (TOF), and promising electrocatalytic activity. [58,59] The major drawback to these approaches is the high synthetic effort and, consequently, the high costs associated with EC fabrication.

This work focuses on the first method described above where an azamacrocycle, in this specific case a TM-containing porphyrin, was mixed with carbon and subject to controlled pyrolysis. Notably, meso-tetraphenyl porphyrins (TPPs) complexing iron(II/III) cations were selected as Fe-containing precursors that were integrated into the carbon matrix through the pyrolytic process. Porphyrins were synthesized from scratch by exploiting the Adler-Longo method, yielding 20 % of the desired product. [60] Roughly 80 % of the original mixture is then considered a waste and is discarded. The poor yield of this synthetic method leads to a high cost of the porphyrins. However, the wastes are complex mixtures containing polypyrromethenes, nitrogen-rich organic compounds that can still chelate metal cations. Hence, it was decided to employ them as valuable precursors to synthesize electrocatalysts.

Importantly, in this work, purified Fe-TPP, unpurified mixture (Fe-TPP/waste) and Fe-waste were studied as precursors to synthesize ORR Fe-N_x type electrocatalysts. In previous works, the addition of a second transition metal to the Fe, especially Mn, in a bimetallic fashion has shown promising results for ORR in an alkaline environment. [39,61] Therefore, Mn-TPP was also synthesized and mixed with Fe-TPP.

The electrocatalysts synthesized were fully characterized from the microscopic and spectroscopic point of view. Moreover, the electrocatalysts were screened from the electrocatalytic perspective to identify their activity. This work shows the possibility of upgrading a waste synthetic process into a valuable and active ORR electrocatalyst.

2. Materials and method

2.1. Organic synthesis

Meso-tetraphenyl porphyrin (meso-TTP) (sample 1; Fig. 1) was prepared according to the well-known Adler-Longo method. [60] Briefly, freshly distilled pyrrole (3.29 mL, 47.7 mmol, Sigma-Aldrich) was rapidly added into a refluxing solution of benzaldehyde (4.84 mL, 47.7 mmol, Sigma-Aldrich) in propionic acid (120 mL, Thermo Fisher) and refluxed in air for 2 h. Afterward, the refluxed solution was cooled to room temperature, and the purple crystalline solid formed (**a**) was filtered, washed 3 × 10 mL with cold methanol, and oven-dried overnight (1.42 g, 2.31 mmol, 19.4 % yield). The black filtrate was instead dried by rotary evaporation and then by high vacuum to afford a black sticky powder named “waste” (sample 2; Fig. 1) (5.90 g).

Later on, the two samples were metallated separately according to the following procedures.

a). Fe-TPP (sample 3, Fig. 2): tetraphenyl porphyrin (sample 1) (100 mg, 0.163 mmol) and iron(II) acetate (28.3 mg, 0.163 mmol, BLD Pharm) were dissolved into 3 mL of anhydrous dimethylformamide (DMF, Acros Organics) under nitrogen atmosphere. The resulting solution was heated at 100 °C for 24 h and the conversion was followed by thin layer chromatography (TLC) with n-Hept/AcOEt 2:1 as eluent. After cooling to room temperature, the mixture was poured into 15 mL of deionized water. The purple precipitate was filtered, washed three times with 5 mL of water, and oven-dried under vacuum overnight (98 mg, 0.147 mmol, quantitative).

b). Fe-Waste (sample 4, Fig. 2): the “waste” (sample 2) (500 mg), derived from the synthesis of sample 1 (TPP), and iron(II) acetate (141.5 mg, BLD Pharm) were dissolved into 15 mL of anhydrous DMF under nitrogen atmosphere. The resulting solution was heated at 100 °C for 24 h. After cooling to room temperature, the mixture was poured into 50 mL of deionized water and extracted with dichloromethane (DCM) (3 × 50 mL). The organic phase was dried with sodium sulfate anhydrous, and the solvent was removed by rotary evaporation to afford a black powder oven-dried under vacuum overnight (490 mg).

c). Mn-TPP (sample 5, Fig. 2): 96 mg of the product was obtained following the same procedure as sample 3 using tetraphenyl porphyrin (sample 1) (100 mg, 0.163 mmol) and manganese(II) acetate tetrahydrate (39.9 mg, 0.163 mmol, Sigma-Aldrich) as reagents.

2.2. Electrocatalysts (EC) fabrication

The suitable amount of metal-nitrogen-containing precursor (samples 3, 4, 5 or their proper mix) was manually blended with the appropriate quantity of Ketjenblack EC-600 JD (KJB, Nanografi) to have an overall ratio of 20 % precursor and 80 % carbon support (1:4 ratio), as summarized in Table 1. The obtained mixture was dispersed in dichloromethane (DCM) using probe sonicator (50 % cycles, 50 % amplitude) for 10 min. Subsequently, the solvent was removed by rotary evaporation and the black powder was oven-dried under vacuum overnight. Afterward, each sample was equally divided into two batches of the same weight, and pyrolysis was performed. For the pyrolysis,

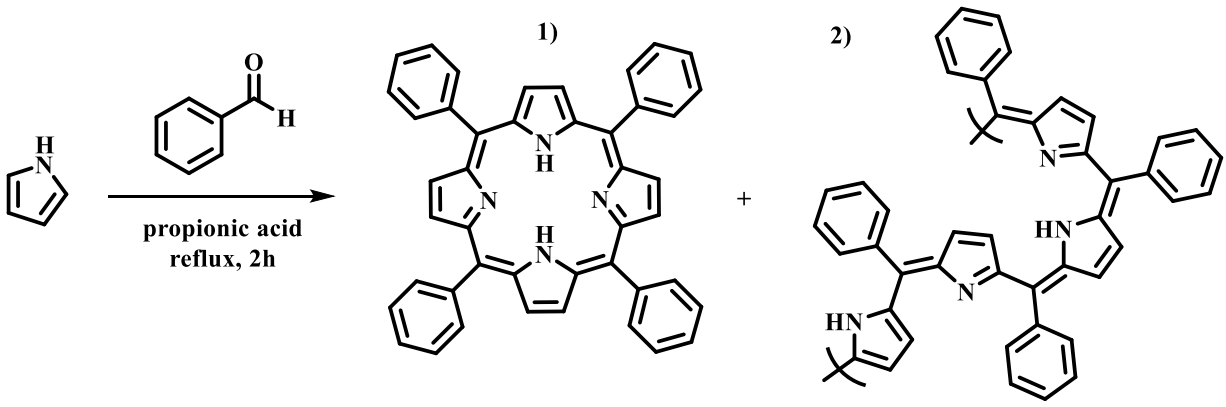

Fig. 1. Adler-Longo synthetic method performed. 1) meso-tetraphenyl porphyrin (TPP), the product of interest; 2) polypyrromethenes, named "waste".

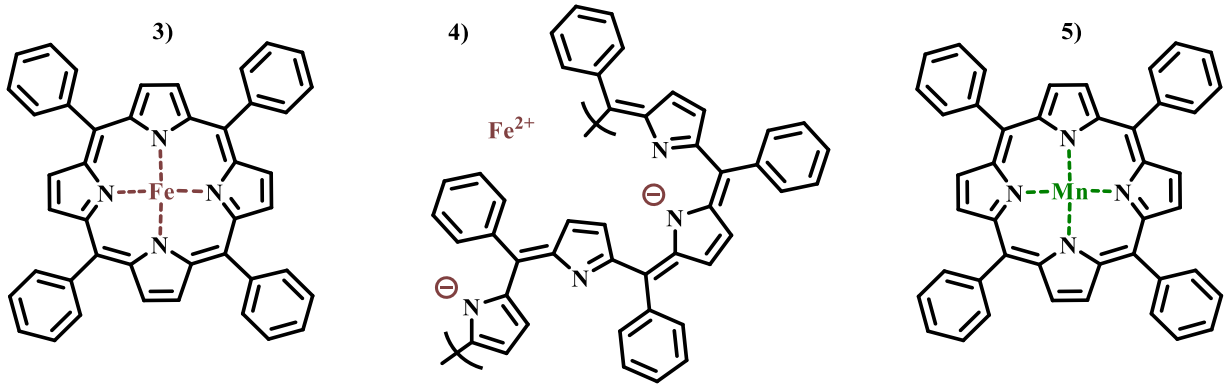

Fig. 2. Iron(II) meso-tetraphenyl porphyrin (Fe-TPP, 3), iron(II) polypyrromethenes (Fe-Waste, 4), and manganese(II) meso-tetraphenyl porphyrin (Mn-TPP, 5) obtained through the metallation process described in Paragraph 2.1.

Table 1
Mixture composition expressed in weight percentage (wt%) and name assigned to the synthesized electrocatalysts. Legend: Fe-TPP: iron(II) meso-tetraphenyl porphyrin (sample 3); Fe-Waste: iron(II) polypyrromethenes (sample 4); Mn-TPP: manganese(II) meso-tetraphenyl porphyrin (sample 5); KJB: Ketjenblack EC-600 JD (Nanografi).

Sample name	Precursors mixture composition (wt%)			
	Fe-TPP	Fe-Waste	Mn-TPP	KJB
FeTPP	20	/	/	80
FeWaste	/	20	/	80
Fe/MnTPP(1:1)	10	/	10	80
FeTPP/Waste(1:4)	4	16	/	80

homogenized mixtures achieved in the previous step were transferred onto an alumina boat and inserted in a quartz tube, equipped with an atmosphere-controlled flange system installed in a horizontal tube furnace (Nabertherm). One batch was pyrolyzed at 600 °C and the other one at 800 °C, both for 1 h (300 °C/hour ramp rates for both heating and cooling) under N_2 atmosphere, after purging the tube with the inert gas for 30 min. All the samples were collected without any significant loss in weight and labeled with the general name: 'Mixture composition_Pyrolysis temperature expressed in Celsius degrees' (e.g., FeTPP_600 for the sample pyrolyzed at 600 °C).

2.3. Electrochemical analysis

The investigation of the oxygen reduction reaction (ORR) electrocatalytic activity of the synthesized samples was conducted employing a rotating ring disk electrode (RRDE) setup, following established methodologies as referenced. [62,63] The experimental setup consisted of a three-electrode configuration system integrating a titanium wire counter electrode, an Ag-AgCl reference electrode (saturated KCl), and an RRDE (E6R2 series, Pine Instruments) serving as the working electrode. The latter was developed by drop-casting the electrocatalyst in the form of ink with 0.2 and 0.6 mg cm^{-2} mass loading on the glassy carbon disk (with an area of 0.2376 cm^2) of the RRDE tip. The ink formulation involved dispersing 5 mg of the EC in a solution comprising 985 μL of isopropanol (Alfa Aesar) and 15 μL of Nafion®d-520 (5 wt%, Alfa Aesar). [62,64] Subsequently, the suspension underwent sonication for 10 min (C 50 %, A 50 %) utilizing a probe sonicator. The assessment of ORR activities was conducted under alkaline conditions using oxygen-saturated 0.1 M $KOH_{(aq)}$ as the working electrolyte.

The study presents all the potential values referenced according to a reversible hydrogen electrode (RHE) using Eq. (1) as follows:

$$E_{RHE} = E_{Ag/AgCl} + E^0{}_{Ag/AgCl} + 0.0591 \cdot pH \quad (1)$$

where $E_{Ag/AgCl}$ is the measured working potential versus Ag/AgCl electrode whereas $E^0{}_{Ag/AgCl}$ is the standard potential of Ag/AgCl reference. pH value is 13 for 0.1 M KOH aqueous solution.

Linear sweep voltammograms (LSVs) at the scan rate of 5 mV s^{-1} were obtained by maintaining the potential window between 1.2 V and 0 V vs RHE while fixing the ring potential of RRDE at 1.2 V vs RHE. The rotation speed was kept at 1600 rpm. Before acquiring actual LSVs, the electrocatalyst was conditioned by applying multiple cyclic voltammetry until a stable behavior was obtained. Finally, peroxide produced (%) and the number of electrons transferred (n) during ORR were calculated by observing the disk current (I_{disk}) and ring current (I_{ring}) as given in Eqs. (2) and (3), respectively. RRDE collection efficiency (N) was 38 %.

$$Peroxide\ (\%) = \frac{200 \cdot \frac{I_{ring}}{N}}{I_{disk} + \frac{I_{ring}}{N}} \quad (2)$$

$$n = \frac{4\ I_{disk}}{I_{disk} + \frac{I_{ring}}{N}} \quad (3)$$

2.4. Advanced characterizations

X-ray diffraction (XRD, Rigaku Miniflex 600) was employed to reveal the crystallographic features of the samples in the 2θ range of 15–80°. The structural integrity of the carbonaceous frameworks was studied through Raman spectroscopical measurements (LabRam, Jobin Yvon, France). He-Ne laser (λ = 632.8 nm) was used to illuminate the samples via microscope (BX40, Olympus, Japan) with an objective lens of 50X (numerical aperture of 0.60) while a silicon CCD (Sincerity, Jobin Yvon, France) was used for the signal collection at 200 K. Energy-dispersive X-ray fluorescence (XRF) having an X-ray tube with a molybdenum anode (Bruker Artax 200 spectrometer) was utilized to perform qualitative elemental analysis.

X-ray photoelectron Spectroscopy (XPS) Analysis through ESCA System PHI 5800 of Physical Electronics X-ray photoelectron spectrometer was employed to investigate the catalysts' surfaces of six samples (FeTPP_600, FeTPP_800, Fe/MnTPP(1:1)_600, Fe/MnTPP(1:1)_800, FeWaste_800 and FeTPP/Waste(1:4)_800). The instrument operates with an Al k_α monochromatic X-ray source at a power of 350 W, and the results were interpreted by a literature study. [65–69]

STEM characterization was performed using a Thermo Fisher Talos F200X G2 TEM, equipped with a four-element EDX detector. Samples were prepared by dropcasting the dispersion of as-developed EC in isopropanol on Cu TEM grids. All the characterizations were performed by using a beam energy of 200 keV.

3. Results and discussion

3.1. Research design

Transition metals-based electrocatalysts of the family of TM-N_x-C are highly active for the ORR, especially in alkaline media. [70,71] Among all the transition metal-nitrogen-containing precursors, iron phthalocyanine (FePc) was widely investigated. [72–76] Concerning other possible interesting substituents, porphyrins were less studied, also due to their associated higher costs (e.g., prices on Sigma-Aldrich website: iron phthalocyanine 65 €/g, iron meso-tetraphenyl porphyrin 394 €/g). [77] Essentially, porphyrins are costly due to both limited market demand and notably low synthetic reaction yields. The Adler-Longo process is the standard and cheapest methodology widely used to synthesize porphyrins. [60] Its yields in moles are around 20 % in the best-case scenario. After the product purification, the remaining mass is considered waste and discarded. However, the latter is mainly composed of polypyrromethenes, molecules with chemical structures that resemble opened porphyrin rings (Fig. 1). Interestingly, both show the same chemical composition and the ability to coordinate metal cations, due to the presence of acidic nitrogen atoms.

This study aims to synthesize porphyrins and their metallated counterpart (Fe and Mn), integrate them into a carbon matrix, and investigate them as TM-N_x-C electrocatalysts. Moreover, the possibility of upcycling the as-considered waste material is shown, aiming at lowering the costs and pursuing a greener approach. Particularly, the electrocatalysts were fabricated by mixing the precursors, including porphyrins and their wastes, with the carbon support (KJB EC-600 JD, Nanografi) and exploiting the pyrolysis approach to embed them into the EC structure. The obtained ORR electrocatalysts were tested in an alkaline environment. The materials and method section comprehensively discusses the fabrication routes and experimental design.

3.2. Structural and morphological investigation

To perform a crystallographic investigation and phase identification, all the developed samples were analyzed through XRD. The achieved diffraction patterns in the 2θ range of 15° to 70° are displayed in Figure S1. All the samples show mainly two peaks at ~25° and ~44° corresponding to (002) and (100) lattices of graphitic carbon, respectively. [62,78,79] This evidence is consistent with what was expected, due to the high ratio of the carbonaceous substrate compared with the N-containing precursors in the synthesized samples. In addition, the ECs FeTPP_800, FeWaste_600, FeWaste_800, and FeTPP/Waste(1:4)_800 exhibit an additional low intense peak at ~35°, ascribable to the diffracting lattices (311) of Fe_3O_4. [80] This suggests the formation of magnetite nanoparticles at higher temperature treatments (e.g. 800 °C), and at lower ones (e.g. 600 °C) if the sample has a high content of FeWaste as TM-N_x source. The evolution and growth of metallic oxide nanoparticles in the metal phthalocyanine-derived electrocatalysts have already been observed during pyrolysis at high temperatures, particularly at or above 600 °C. [37,49] This evidence is confirmed by the STEM analysis displayed later on in Section 3.3.

Involving the Raman spectroscopy, it is possible to further investigate the carbonaceous structure of the synthesized electrocatalysts. As known from the literature, there are two typical absorption bands peculiar to carbon-based materials: G (nearly 1580 cm^{-1}) and D (nearly 1310 cm^{-1}), associated with in-plane stretching of the sp^2 carbon atom with E_{2g} symmetry and breathing mode of A_{1g} symmetry, respectively. [81–83] To summarize, the G band manifests the level of graphitization, and the D band the induced defects in the original lattice or the edge of graphene crystals. As it is well known, the ratio of D to G band intensity (I_D/I_G) manifests the degree of disorder in carbon-based materials. All the synthesized samples show values of I_D/I_G higher than one, around 1.3, which indicates the occurrence of a very high defect density (Figure S2, Table S1). High defect density can boost the ORR activity due to the modified electronic and chemical characteristics of the disrupted carbons. [84] Interestingly, the ratio I_D/I_G increases after the pyrolysis treatment (1.06 for pristine KJB), suggesting that the heat treatment induces structural changes and defectivity also at the carbon matrix level.

Qualitative elemental analysis was carried out using XRF (Figure S3). The starting material before the pyrolysis is the same for both the heat-treated samples at 600 °C and 800 °C, therefore only the 600 °C samples were analyzed. Each collected spectra show clearly the peaks of the metal of interest, i.e. Fe and/or Mn, justifying the effectiveness of the synthetic process.

3.3. Surface and bulk characterization

It was shown that the surface chemistry of the electrocatalysts plays a crucial role in the electrocatalytic activity and the mechanisms that take place. [30] Therefore, XPS was used to identify the surface composition of the synthesized electrocatalysts. Table 2 displays the surface composition derived from the survey spectra of FeTPP_600, FeTPP_800, Fe/MnTPP(1:1)_600, Fe/MnTPP(1:1)_800, FeWaste_800 and FeTPP/Waste(1:4)_800 electrocatalysts. XPS spectra indicate the presence of

Table 2
Atomic percentage of C1s, N1s, Fe2p3, Mn2p3, and O1s in the electrocatalysts derived from XP survey spectra.

Sample Name	Carbon C1s	Nitrogen N1s	Iron Fe2p3	Manganese Mn2p3	Oxygen O1s
FeTPP_600	98.0	0.5	0.2	–	1.3
FeTPP_800	96.5	0.3	0.1	–	3.1
FeWaste_800	96.8	0.5	0.1	–	2.8
Fe/MnTPP(1:1)_600	94.8	0.9	0.1	0.1	4.1
Fe/MnTPP(1:1)_800	94.5	0.6	0.1	0.1	4.7
FeTPP/Waste(1:4)_800	97.6	0.5	0.1	–	1.8

carbon, nitrogen, iron and/or manganese, and oxygen. The most prevalent species in all these compounds is C1s, whose atomic percentage ranges from 94.5 % for Fe/MnTPP(1:1)_800 to 98 % for FeTPP_600. The catalysts' surface is also characterized by a low nitrogen content (<1 %), mainly for the catalysts treated at the highest temperature, and by remarkably low amount of metal (<0.3 %).

The signals of five distinct nitrogen species were taken into consideration for N1s deconvolution even if the spectra in Fig. 3 appear scattered for the low nitrogen atomic percentage: imine at 397.5 ± 0.1 eV, pyridinic-N at 398.4 ± 0.1 eV, Nx-M (*M*=Fe, Mn) at 399.7 ± 0.1 eV, pyrrolic-N at 400.8 ± 0.1 eV, and graphitic-N at 402.3 ± 0.1 eV. As reported in Table 3, FeTPP_600 has the largest pyridinic/pyrrolic content followed by FeTPP_800. The most significant interaction between N-moieties and the metals (*M*=Fe, Mn) was exhibited by FeWaste_800 with a relative percentage of 35.5 % ± 0.1. Instead, the other catalysts are characterized by a similar N-M relative percentage ranging between 20.2 % and 24.1 %.

The deconvolution of C1s spectra and the corresponding compositional analysis are shown in Fig. 4 and Table 4, respectively. The binding energy for graphitic carbon is 284.3 eV; for secondary carbons coordinated to carbon-nitrogen or carbon-oxides it is 285.0 eV; whereas CNx defects appear at 286.2 eV; alcohol and ether groups (C—OH/C—OC) at 287.1 eV; ketones or aldehydes (C = O) at 288.1 eV and COOH at 289.5 eV. FeTPP_600 has the highest concentration of graphitic carbon, followed by FeTPP/Waste(1:4)_800 and FeWaste_800. Regarding C—N defects, all the catalysts treated at 800 °C are characterized by a slightly larger content than the catalysts heat-treated at 600 °C. FeWaste_800 exhibits the largest relative percentage of C—N defects (11.8 %), whereas the other catalysts are characterized by C—N defects ranging between 8.8 and 9.9 %.

STEM-EDX was performed on the samples to highlight the presence of nanoparticles in the various samples (Fig. 5). Interestingly, for the samples in which only Fe is present, nanoparticles appeared only after the 800 °C heat treatment, while the addition of Mn seems to hinder nanoparticle formation at the same temperature. The FeTPP_800 catalyst contains rounded particles with diameters in the range of 20–25 nm, while the waste retains smaller and more dimensionally dispersed entities.

3.4. ORR electrocatalytic activity in alkaline media

The synthesized materials described in the present work were investigated for ORR in alkaline media (O_2-saturated 0.1 M KOH) through the RRDE experiment. The results shown in this section refer to a catalyst loading of 0.6 mg cm^{-2}. As suggested by the literature, a thicker electrode lowers the peroxide production and increases the kinetics. [85–87] The same trend was observed in this work. The comparison between 0.2 and 0.6 mg cm^{-2} loading for the catalysts FeTPP_600 and FeTPP/Waste(1:4)_800 is shown in the Supporting Material (Figure S4 and S5), along with the durability testing for FeTPP_600 (Paragraph SP1 and Figure S6).

Remarkably, all the samples demonstrated appreciable electrocatalytic activity towards ORR electrocatalysis. For comparison, all the performance descriptors are reported in Table 5. From the LSVs presented further (Figs. 6a, 7a, and 8 a), ORR kinetics launched by the ECs can be appreciated. In general, the onset potential (E_{onset}) is above 0.94 V vs RHE (and the overall range is from 0.94 to 1.01 V vs RHE), the halfway potential ($E_{1/2}$) is above 0.82 V vs RHE (ranging from 0.82 to 0.88 V vs RHE) and the limiting current (J_{lim}) at 0 V vs RHE varied between 3.17 and 6.4 mA cm^{-2}. The electrocatalytic activity is generally high and the higher performance is in line with the activity of the Pt/C electrocatalysts. [88] Furthermore, from the J_{ring} (Figs. 6b, 7b, and 8b), it is possible to calculate the percentage of peroxide produced and the number of electrons transferred. For FCs, it is pivotal to minimize the peroxide yield while promoting the direct tetra-electronic ORR. [30,89] The synthesized ECs produced a low content of peroxide, quantified below 14 % (Figs. 6c, 7c and 8c). It was noticed that peroxide increased with the increased overpotentials. Furthermore, a high number of electrons transferred, above 3.7 electrons was observed (Fig. 6d, 7d, and 8d). Both the data are quite promising, and it is possible to speculate a direct 4 and a 2 × 2 electron transfer mechanism. Indeed, due to the low peroxide, the majority of the oxygen is reduced to the final product without intermediates. Moreover, the low peroxide indicates the presence of active sites of the type Fe-N_x-C responsible for the direct 4 electrons transfer. Secondary active sites, nitrogen-pyridinic, less active but more selective can contribute to reducing the intermediate to the final product, reducing the peroxide detected. [90]

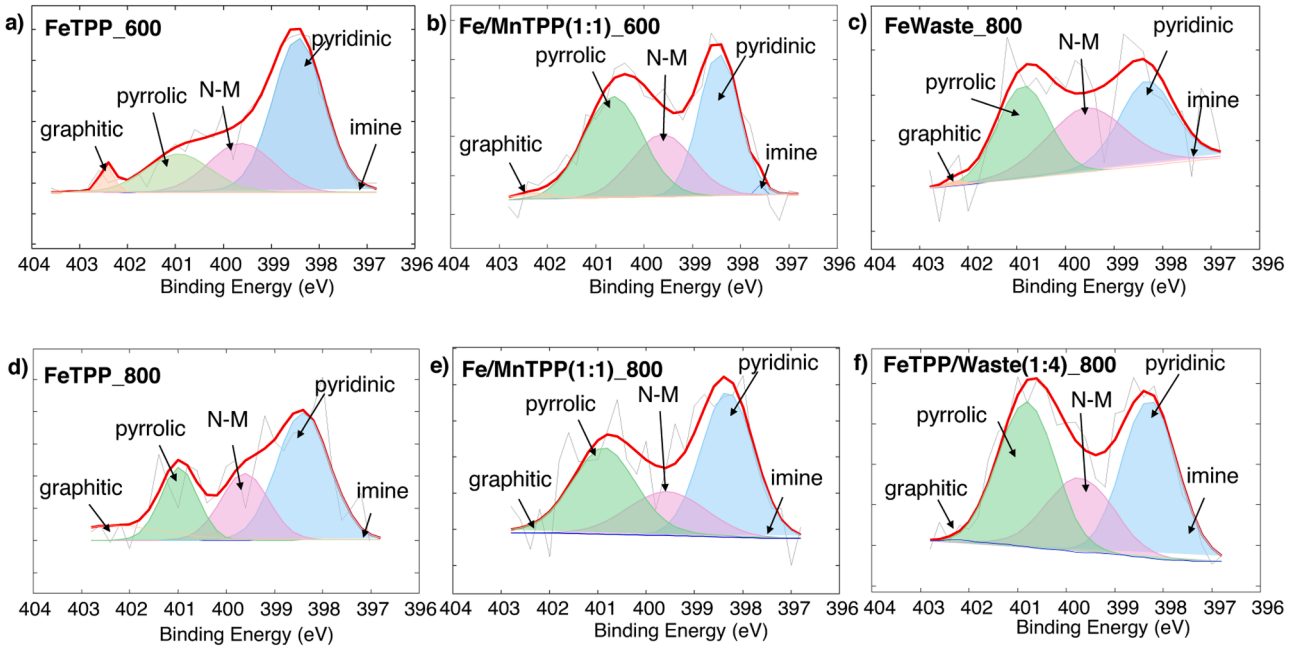

Fig. 3. Comparison of XPS N1s signals for FeTPP treated at a) 600 °C (FeTPP_600) or d) 800 °C (FeTPP_800); Fe/Mn-TPP treated at b) 600 °C (Fe/MnTPP(1:1)_600) or e) 800 °C (Fe/MnTPP(1:1)_800); c) FeWaste_800 and f) FeTPP/Waste(1:4)_800.

Table 3
Nitrogen speciation from N1s deconvolution spectra.

Composition of N (relative %)						
Sample Name	N, (at. %)	Imine, (397.5 eV)	Pyridinic, (398.4 eV)	Nx-M, (*M*=Fe, Mn), (399.7 eV)	Pyrrolic (400.8 eV)	Graphitic, (402.3 eV)
FeTPP_600	0.5	0	57.6	21.9	18.0	2.5
FeTPP_800	0.3	0	48.3	22.5	19.0	10.2
FeWaste_800	0.5	0	32.9	35.4	31.1	0.6
Fe/MnTPP(1:1)_600	0.9	0.2	36.1	24.1	38.2	1.4
Fe/MnTPP(1:1)_800	0.6	0	44.8	20.2	35	0
FeTPP/Waste(1:4)_800	0.5	0	39.3	22.6	37.7	0.4

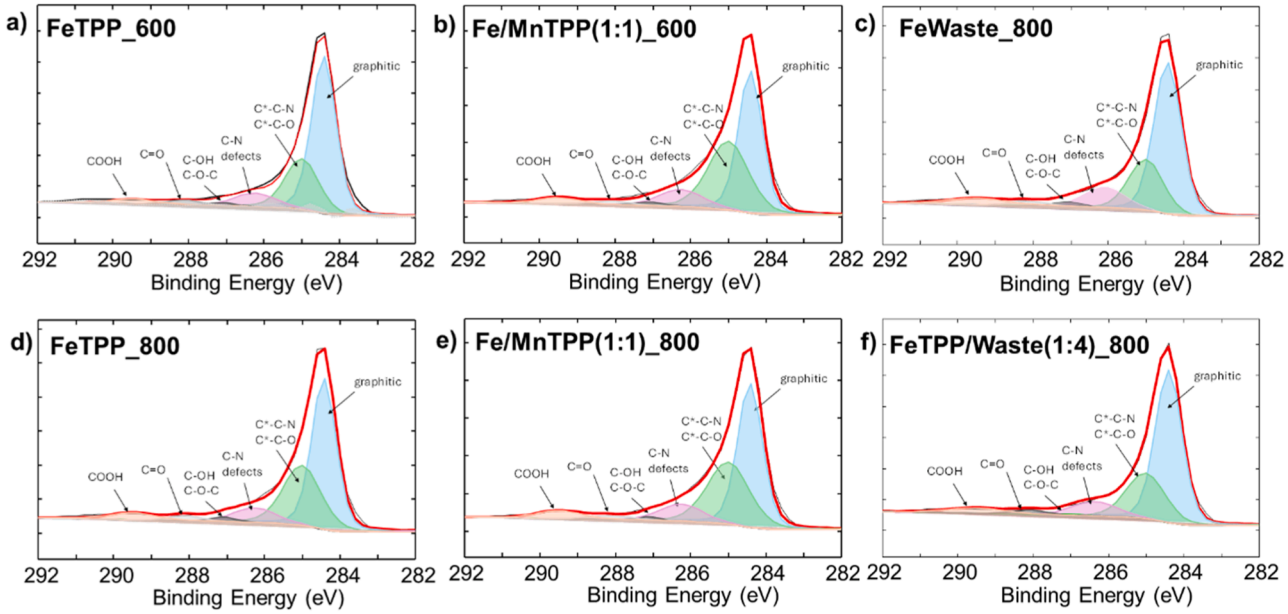

Fig. 4. Comparison of XPS C1s signals for FeTPP treated at a) 600 °C (FeTPP_600) or d) 800 °C (FeTPP_800); Fe/MnTPP treated at b) 600 °C (Fe/MnTPP(1:1)_600) or e) 800 °C (Fe/MnTPP(1:1)_800); c) FeWaste_800 and f) FeTPP/Waste(1:4)_800.

Table 4
Carbon speciation from C1s deconvolution spectra.

Composition of C (relative %)							
Sample Name	C (at. %)	Graphitic (284.3 eV)	Secondary carbons (285.0 eV)	C-Nx defects (286.2 eV)	C—OH/C—OC (287.1 eV)	C = O (288.1 eV)	COOH (289.5 eV)
FeTPP_600	98	58.6	25.7	8.8	1.1	3.5	2.3
FeTPP_800	96.5	51.2	31.5	9.1	1.3	4.4	2.5
FeWaste_800	96.8	55.5	23.1	11.8	2	5.6	2
Fe/MnTPP(1:1)_600	94.8	45.9	37.3	9.8	1.3	3.9	1.8
Fe/MnTPP(1:1)_800	94.5	47.7	34.6	9.9	0.9	4.7	2.2
FeTPP/Waste(1:4) _800	97.6	58.3	24.9	9.2	0.7	5.0	1.9

3.4.1. Effect of temperature treatment on ORR electrocatalytic activity

Firstly, the pyrolysis temperature (T) was varied to evaluate the effects on the electrocatalytic activity depending on the nature of the pyrolyzed material (Fig. 6). Two temperatures, 600 °C and 800 °C, were chosen according to the latest literature results. [49] Pure iron(II) porphyrin mixed with carbon pyrolyzed at 600 °C (FeTPP_600) showed higher values of E_{onset} and $E_{1/2}$ compared with the values obtained for the sample treated at 800 °C (FeTPP_800; Table 5 Entries 1–2). Also, the percentage of peroxides for FeTPP_600 is lower and the number of electrons transferred is close to being equal to four. Interestingly, contrary results were obtained by pyrolyzing the FeWaste supported on carbon. In this case, higher temperature treatments (e.g., 800 °C) generate higher electrocatalytic activity in terms of E_{onset}, $E_{1/2,}$ and J_{limit} but slightly worse results in terms of peroxide production and electrons transferred (Entries 3–4). Moreover, this trend is confirmed by evaluating the electrocatalytic activity of the samples FeTPP/Waste(1:4) (Entries 5–6). It is worth noticing that this sample is mainly composed of "waste" precursor, simulating the true composition of the mixture before porphyrin purification, therefore the behavior is aligned with the LSV results described above for the FeWaste_800 sample. Nevertheless, the mixed EC contains a small percentage of porphyrin, which helps decrease the peroxide production and increase the electrons transferred compared to the FeWaste_800 sample, reaching values comparable to FeTPP_800.

3.4.2. Effect of the addition of the second transition metal on ORR electrocatalytic activity

It was previously shown in the literature that the addition of Mn as

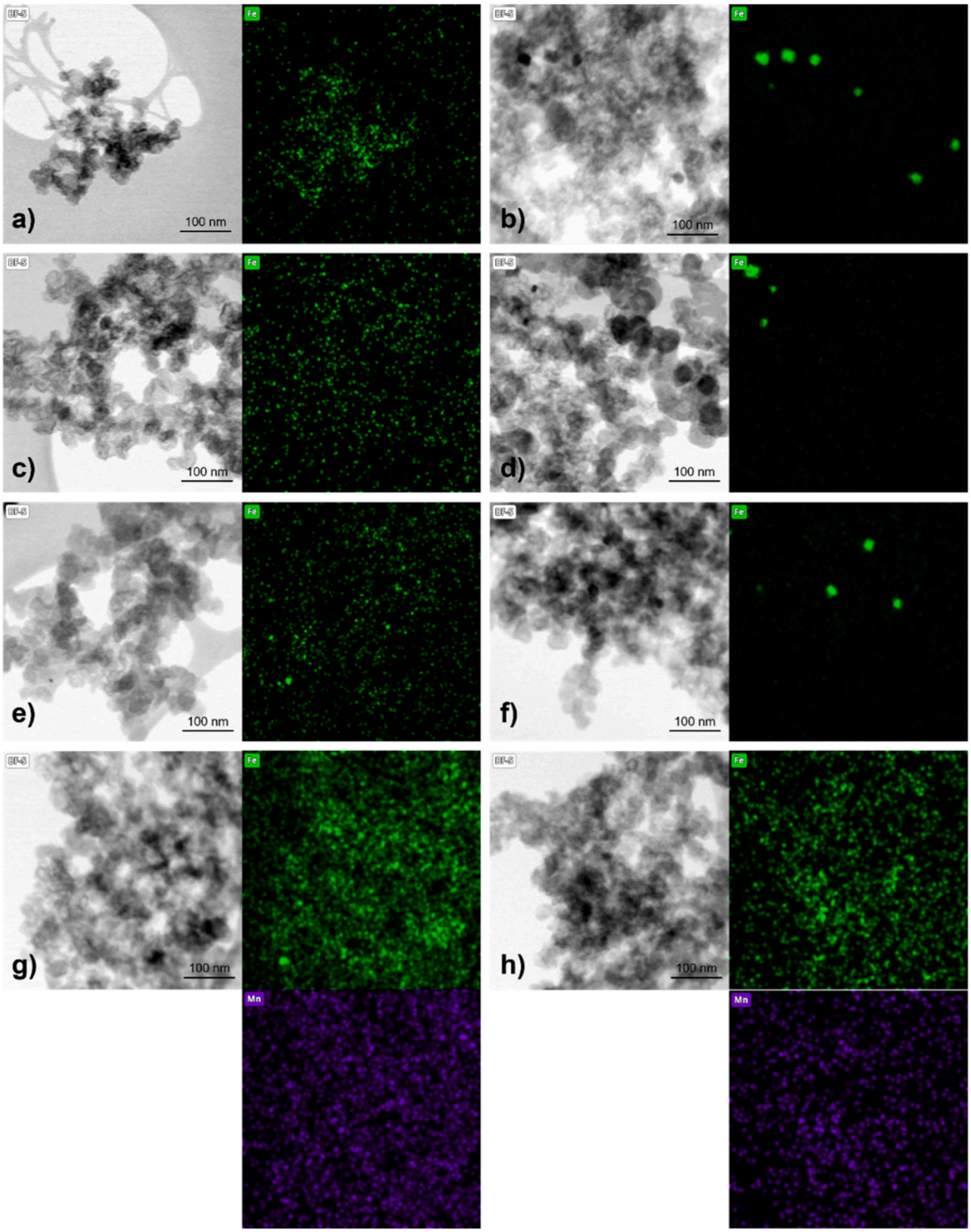

Fig. 5. STEM and EDX images of the samples: leftmost column related to the samples treated at 600 °C, rightmost column related to 800 °C samples. Label a) and b) FeTPP, c) and d) FeWaste, e) and f) FeTPP/Waste(1:4), g) and h) Fe/MnTPP(1:1).

Table 5
Electrochemical results of the synthesized ECs experimentally obtained by rotating ring disk electrode (RRDE) setup applied for the oxygen reduction reaction (ORR) in alkaline media (0.1 M KOH(aq)).

Entry	Sample Name	E_{onset} (V vs RHE)	$E_{1/2}$ (V vs RHE)	$J_{limiting}$ (mA cm^{-2})	% peroxide at 0 V vs RHE	n° of e^- transf. at 0 V vs RHE
1	FeTPP_600	0.972	0.852	−6.33	1.9	3.96
2	FeTPP_800	0.952	0.872	−4.45	6.6	3.87
3	FeWaste_600	0.937	0.830	−3.17	9.9	3.80
4	FeWaste_800	1.007	0.842	−3.32	11.7	3.76
5	FeTPP/Waste (1:4)_600	0.952	0.861	−3.66	14.3	3.71
6	FeTPP/Waste (1:4)_800	0.977	0.853	−4.38	8.3	3.83
7	Fe/MnTPP (1:1)_600	0.957	0.817	−5.50	4.9	3.90
8	Fe/MnTPP (1:1)_800	0.977	0.879	−4.59	8.3	3.84

co-metal to Fe has a positive effect on ORR. [39,91,92] Therefore, the electrocatalytic activity of the synthesized materials was also evaluated after the addition of Mn. However, this strategy does not significantly improve the electrocatalytic performances. As shown in Fig. 7 and summarized in Table 5 Entries 7–8, the samples pyrolyzed at 600 °C exhibit some differences, especially in terms of the LSV results. Indeed, the measured values for FeTPP_600 and Fe/MnTPP(1:1)_600 were 0.972 and 0.957 V vs RHE for E_{onset}, and 0.852 and 0.817 V vs RHE for $E_{1/2}$, respectively. Furthermore, the results regarding peroxide production and number of electrons transferred worsen for the Mn-containing sample. Concerning the ECs pyrolyzed at 800 °C, neither significant changes in LSV results can be appreciated, nor in terms of the overall kinetic reduction mechanism. It is possible to conclude that, in this work, the addition of Mn as a co-metal to Fe is redundant.

3.4.3. *Effect of the presence of synthetic waste on ORR electrocatalytic activity*

A final, pivotal, consideration should be done about employing also the waste material of the porphyrin synthesis to fabricate ORR electrocatalysts. As shown in Fig. 8, the E_{onset} and the $E_{1/2}$ of FeTPP_600 and FeTPP/Waste(1:4)_800 are essentially equal (0.97 and 0.85 V vs RHE, respectively; see Table 5, Entries 1 and 6), manifesting good kinetics for both ECs. However, the limiting current of the latter is two points lower than the one of the former (4.38 and 6.33 mA cm^{-2}, respectively), displaying lower activity for the diffusion regime. Concerning the peroxide production and the number of electrons transferred, both materials show good results, keeping the values below 8 % and above 3.8, respectively. On the contrary, the sample obtained exclusively from the functionalized waste material (FeWaste_800, Table 5, Entry 4) exhibits slightly worse catalytic performances. Its kinetics regime is as good as the two previously discussed ECs (E_{onset} = 1.077 V vs RHE; $E_{1/2}$ = 0.842 V vs RHE), but its diffusion one is not (3.32 mA cm^{-2}). The peroxide production is near 12 % and the trend of electrons transferred is above 3.75.

These results endorse the idea of exploiting the unpurified

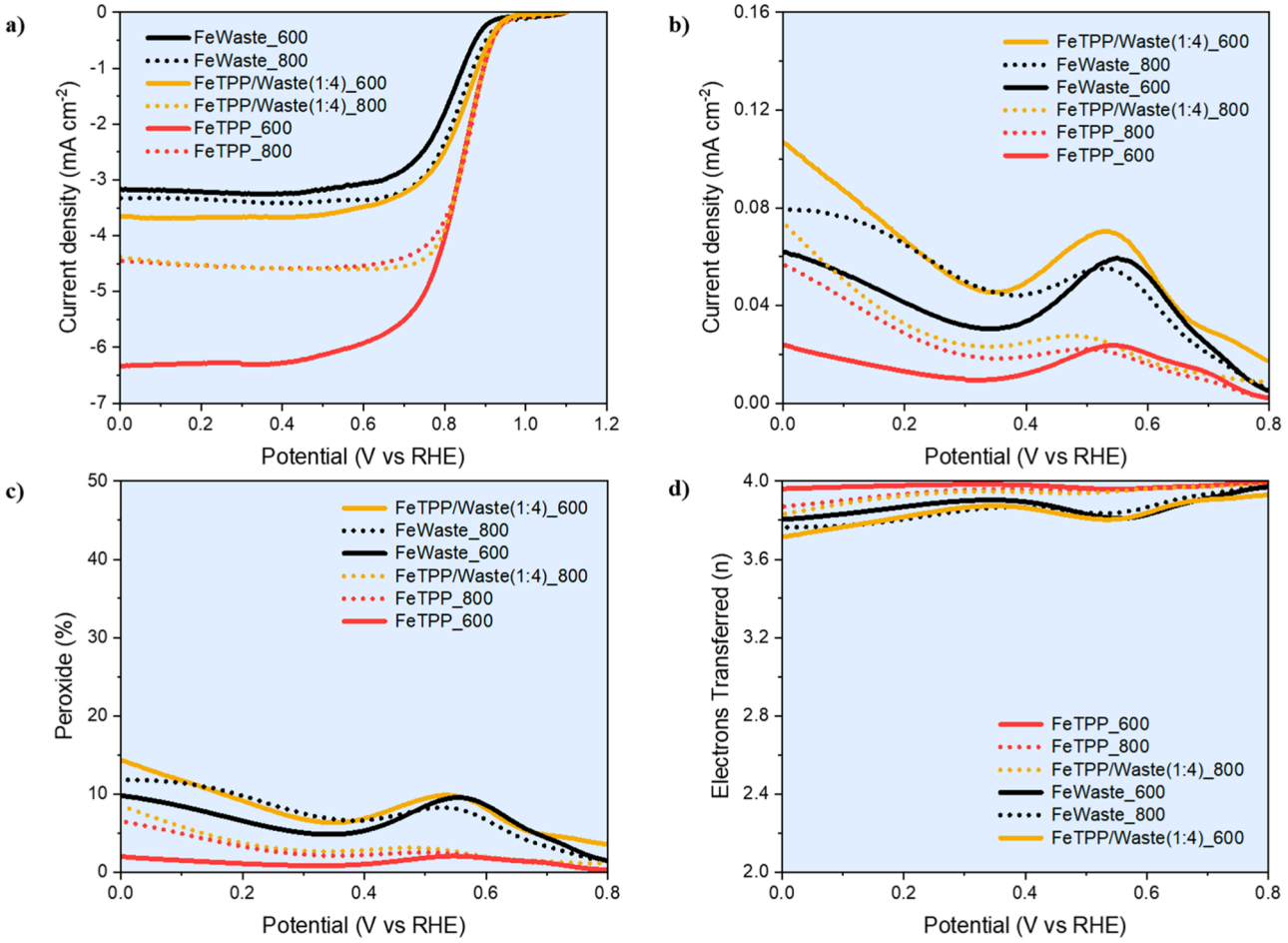

Fig. 6. Effect of temperature treatment on ORR electrocatalytic activity of the synthesized ECs (0.6 mg cm^{-2} loading in 0.1 M KOH, oxygen saturated) recorded with an RRDE setup at 1600 rpm. a) linear sweep voltammetry (LSV) at 5 mV s^{-1}; b) ring current densities; c) trends of produced peroxide; d) trends of the electrons transferred.

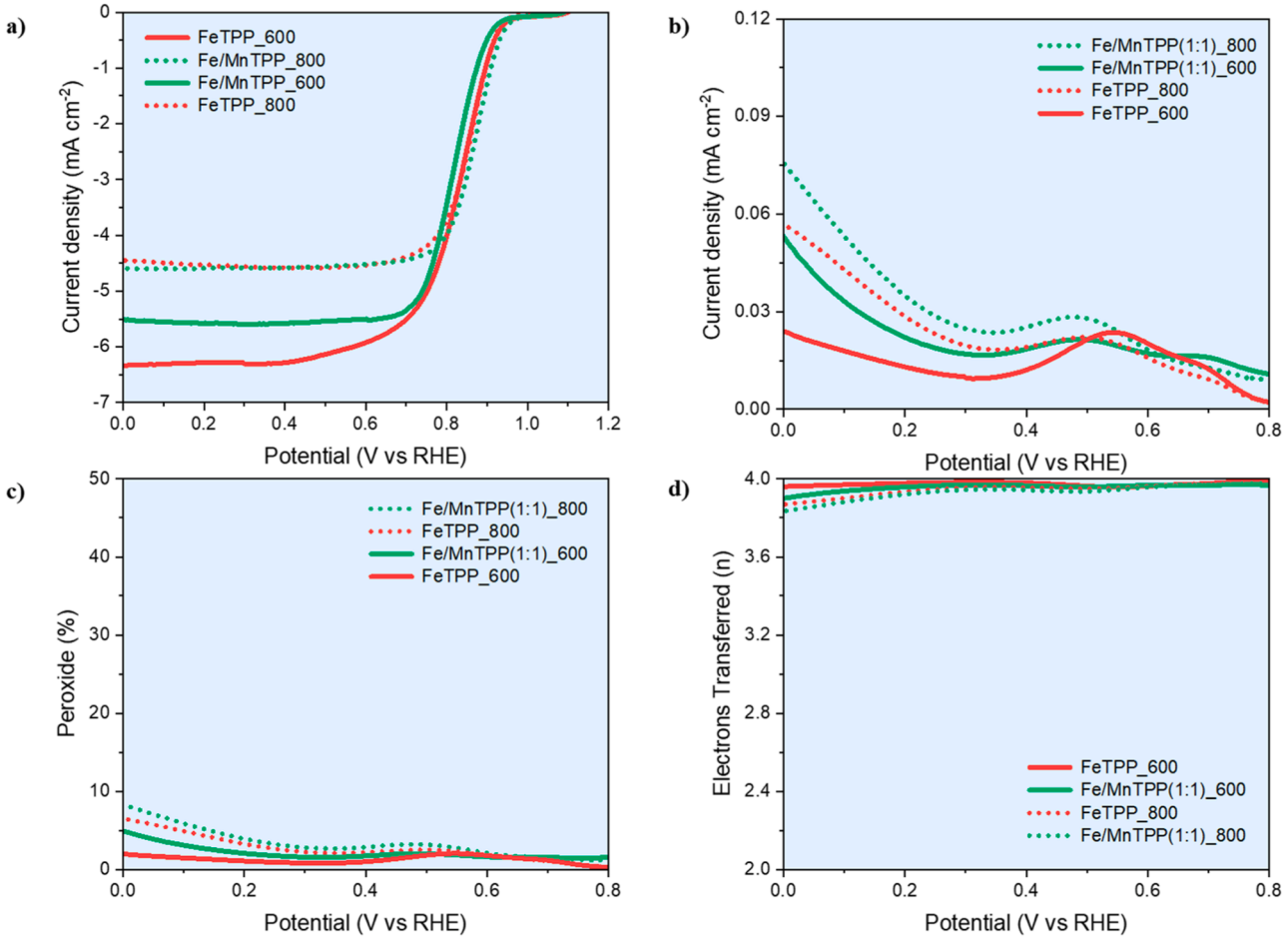

Fig. 7. Effect of the addition of the second transition metal on ORR electrocatalytic activity of the synthesized ECs (0.6 mg cm^{-2} loading in 0.1 M KOH, oxygen saturated) recorded with an RRDE setup at 1600 rpm. a) linear sweep voltammetry (LSV) at 5 mV s^{-1}; b) ring current densities; c) trends of produced peroxide; d) trends of the electrons transferred.

porphyrins as N-containing precursors to fabricate ECs. Following this approach, good electrocatalytic performance could be achieved, significantly lowering the process costs. Therefore, it could be a good strategy to exploit the crude mixture TPP/Waste (about 20:80 wt%) to fabricate good electrocatalysts for ORR in an alkaline environment.

3.4.4. Remarkable considerations on ECs ORR activity

The selective ORR activity is influenced by the active site structures that evolve during the synthesis of the electrocatalyst. Since TM-N_x-C are composed of numerous active moieties and each of them contributes differently, the overall performance is a cumulative response determined by the proportion and distribution of the primary and secondary active sites. [30,93,94] It is well known in the community that the atomically dispersed TM-N_x (x = 2–4) are the primary active sites to launch a direct 4-electron ORR pathway. [95,96] Whereas pyrrolic and pyridinic nitrogen act as secondary active sites. The former is responsible for the two-electronic reduction of O_2 into peroxide while the latter stepwise converts the produced peroxides into water and completes the reaction. [97,98] It is also important to highlight that the coalescence of metallic species into nanoparticles not only affects the kinetic activity but also increases the peroxide yield [49,67,99] and similarly the higher content of graphitic nitrogen is linked with performance decay (lowering the E_{on} and $E_{1/2}$) and higher peroxide yield. [100,101] Quite interestingly, the sample FeTPP_600, fabricated with pure Fe porphyrin, demonstrated higher E_{onset} and $E_{1/2}$ together with peak $J_{limiting}$. Moreover, the same sample exhibited an amazingly low peroxide yield while maintaining the direct 4e ORR. Such a remarkable performance can be attributed to a suitable combination of higher pyridinic content and lower graphitic nitrogen along with the absence of metallic nanoparticles as confirmed by the HRTEM analysis. On the other hand, increasing the pyrolysis temperature from 600 to 800 °C not only gave rise to the evolution of nanoparticles but also increased graphitic nitrogen while reducing the pyridinic nitrogen in the derived sample i.e. FeTPP_800. This could be a reason behind the relative performance degradation observed in the case of FeTPP_800. Notably, the enhanced E_{onset} and $E_{1/2}$ of FeWaste_800 could result from a higher proportion of TM-N_x sites but the higher peroxide yield could be due to the presence of metallic nanoparticles and excess pyrrolic nitrogen. Contrary to previous research on bimetallic electrocatalysts, the Fe/MnTPP samples didn't show any significant difference from the monometallic samples, however, the slight decay can be stemmed from higher pyrrolic nitrogen and lower pyridinic nitrogen content. Nonetheless, it is crucial to note that the waste-derived electrocatalysts exhibited similar structural attributes and consequently comparable performance metrics. These observations support the lucid idea of repurposing the waste generated during the synthesis of porphyrins in the production of efficacious TM-N_x-C.

4. Novelty and take-home message

The atomic level coordination between TM (in monometallic or bimetallic configuration) with nitrogen i.e. TM-N_x is essentially important to produce primary active sites for the ORR electrocatalysis while replacing the scarce and expensive PGMs, particularly in the alkaline

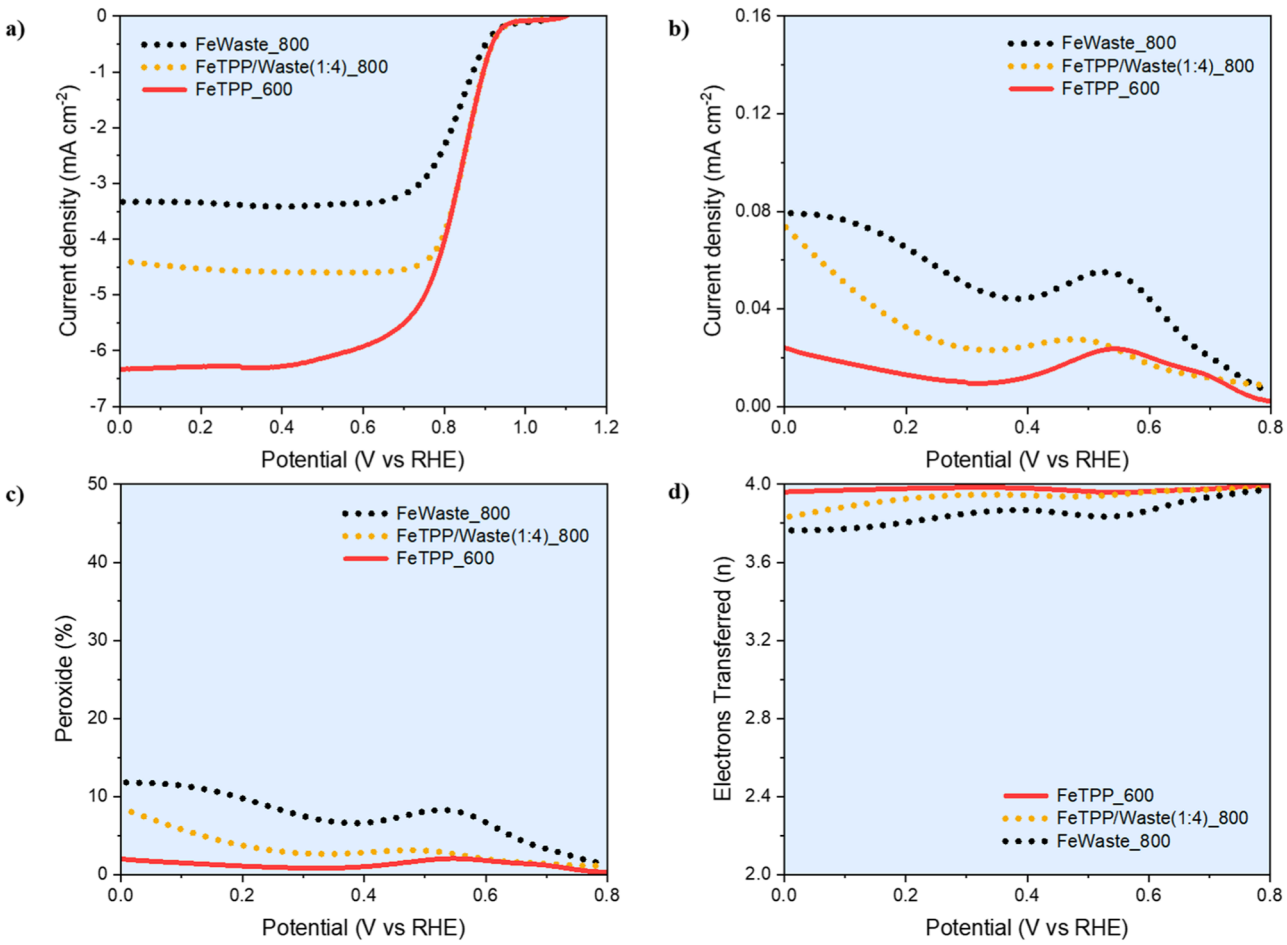

Fig. 8. Effect of the presence of synthetic waste on ORR electrocatalytic activity of the synthesized ECs (0.6 mg cm^{-2} loading in 0.1 M KOH, oxygen saturated) recorded with an RRDE setup at 1600 rpm. a) linear sweep voltammetry (LSV) at 5 mV s^{-1}; b) ring current densities; c) trends of produced peroxide; d) trends of the electrons transferred.

medium. Such configuration already exists in the aza-macrocycles such as phthalocyanine (Pc), porphyrins, etc. and hence they carry out oxygen electro-reduction while bio-mimicking the natural enzymes such as cytochrome c oxidase and ubiquinol oxidase. [70] In the paradigm of aza-macrocycles for ORR, FePc is one of the most popular candidates owing to suitable electronic configuration and Fe(III)/(II) formal redox potential. [102] However, the planar symmetric Fe-N_4 sites in FePc lead to inadequate ORR activity due to its inferior O_2 adsorption and reduction and therefore require structural substitutions and redesigning. [72,103,104] On the other hand, porphyrins are another promising competitor to improve the cathodic reaction of FCs. [105–108] In any case, both types of chelated metal macrocyclic have to be embedded in a carbonaceous framework via pyrolysis to improve structural stability. [109,110] During pyrolysis, the structural parameters, coordination chemistry, and active sites go on transforming depending on the pyrolysis conditions i.e. temperature, and hence original configuration may be lost. [37,49,111].

Despite being an excellent TM-N_x source, porphyrins are relatively less studied for this purpose because they are much more expensive compared to Pc. The low synthetic yield (around 20 % involving the Adler-Longo procedure) is one of the major drawbacks regarding these organic compounds. Importantly, the huge amount of waste (around 80 % of the total mass) produced by the synthetic process contains nitrogen that can coordinate metal cations. This consideration is pivotal in pursuing a greener approach to fabricating new ECs. Recently, following the theme of *Circular Economy* waste-derived TM-N_x-C type electrocatalysts have acquired significant attention where organic wastes (plastics and biomasses) have been utilized as a carbon source but still nitrogen and metal precursors are required to induce the active moieties. [112–116] The residue of porphyrin synthesis can resolve this problem. Instead of the direct employment of expensive pure porphyrins, the generated chemical waste can itself be utilized for the realization of efficacious electrocatalysts of ORR. Following similar concepts, such as integration with high surface carbons and/or introducing a secondary metal source, i.e. Mn or other metals, during pyrolysis can provide a strategic pathway to enhancing the selective activity and operative robustness. In this consideration, the presented study coines the notion of repurposing the discarded porphyrin wastes in the fabrication of the electrocatalysts. Finding a suitable pyrolysis temperature and the proportion of the precursors (both pure and waste-derived) can dictate the surface chemistry and morphology evolved to ensure appreciable ORR performance. Anyhow, the remarkable electrocatalytic performance exhibited by the fabricated electrocatalyst justifies the intellectual approach of this study and of course, the prospective endeavors can further improve the kinetic performance of waste-derived electrocatalysts.

5. Conclusions

The presented work demonstrated the possibility of using transition metal porphyrins, particularly based on iron, as organic, metal-containing precursors for the synthesis of ORR-active ECs. Moreover, the possibility of integrating the discarded porphyrin synthetic waste into the active electrochemical material was presented. This strategy allowed the upcycling of the waste and unused material for porphyrin

synthesis, increasing the overall sustainability of the final ECs. Remarkably, the sample made using purified porphyrin precursor and pyrolyzed at 600 °C (FeTPP_600) showed the best performance in terms of overall linear sweep voltammetry metrics (0.972 and 0.852 V vs RHE for E_{onset} and $E_{1/2}$, respectively; - 6.33 mA cm^{-2} for $J_{limiting}$) and direct four-electron reduction pathway. Nevertheless, the sample obtained by mixing porphyrins with their synthetic waste in the ideal ratio of 1:4 and pyrolyzed at 800 °C (FeTPP/Waste(1:4)_800) still exhibits appreciable kinetics results but less efficient diffusion regime (0.977 and 0.853 V vs RHE for E_{onset} and $E_{1/2}$, respectively; - 4.38 mA cm^{-2} for $J_{limiting}$). Nevertheless, the obtained results are encouraging for both the materials and open the possibility of utilization of unpurified porphyrins in ECs development for ORR, at ultra-low loading of atomically dispersed transition metal (0.2 atomic % of iron on the sample FeTPP _600, XPS results).

CRediT authorship contribution statement

Nicolò Giulini: Writing – review & editing, Writing – original draft, Methodology, Investigation, Formal analysis, Data curation, Conceptualization. **Mohsin Muhyuddin:** Writing – review & editing, Writing – original draft, Funding acquisition, Formal analysis, Data curation, Conceptualization. **Sara Mattiello:** Writing – review & editing, Writing – original draft, Methodology, Formal analysis, Data curation. **Mauro Sassi:** Writing – review & editing, Writing – original draft, Methodology, Investigation, Formal analysis. **Carmelo Lo Vecchio:** Writing – review & editing, Writing – original draft, Methodology, Investigation, Formal analysis, Data curation. **Vincenzo Baglio:** Writing – review & editing, Writing – original draft, Methodology, Investigation, Formal analysis. **Enrico Berretti:** Writing – review & editing, Writing – original draft, Investigation, Formal analysis, Data curation. **Alessandro Lavacchi:** Writing – review & editing, Writing – original draft, Investigation, Formal analysis, Data curation. **Enza Fazio:** Writing – original draft, Investigation, Formal analysis, Data curation. **Luca Beverina:** Writing – review & editing, Writing – original draft, Supervision, Project administration, Methodology, Investigation, Funding acquisition, Conceptualization. **Carlo Santoro:** Writing – review & editing, Writing – original draft, Supervision, Project administration, Investigation, Funding acquisition, Conceptualization.

Declaration of competing interest

The authors declare that they have no known competing financial interests or personal relationships that could have appeared to influence the work reported in this paper.

Data availability

Data will be made available on request.

Acknowledgments

M.M., C.S. and A.L. would like to acknowledge the Cariplo Foundation Call for Circular Economy through the project “Transformation of plastic waste in Electrocatalysts, Supported by exhausted gases recovery Layout” (TESLA).

Supplementary materials

Supplementary material associated with this article can be found, in the online version, at doi:10.1016/j.electacta.2024.145113.

References

[1] A. Boudghene Stambouli, E. Traversa, Fuel cells, an alternative to standard sources of energy, Renew. Sustain. Energy Rev. 6 (2002) 295–304, https://doi.org/10.1016/S1364-0321(01)00015-6.
[2] U.S.D. of E. NETL, Fuel Cell Handbook (7th Edition), (2004). https://netl.doe.gov/search/node?keys=FC%20Handbook%207.
[3] X. Ren, Q. Lv, L. Liu, B. Liu, Y. Wang, A. Liu, G. Wu, Current progress of Pt and Pt-based electrocatalysts used for fuel cells, Sustain. Energy Fuels 4 (2020) 15–30, https://doi.org/10.1039/C9SE00460B.
[4] X. Ren, Y. Wang, A. Liu, Z. Zhang, Q. Lv, B. Liu, Current progress and performance improvement of Pt/C catalysts for fuel cells, J. Mater. Chem. A 8 (2020) 24284–24306, https://doi.org/10.1039/D0TA08312G.
[5] L. Huang, S. Zaman, X. Tian, Z. Wang, W. Fang, B.Y. Xia, Advanced platinum-based oxygen reduction electrocatalysts for fuel cells, Acc. Chem. Res. 54 (2021) 311–322, https://doi.org/10.1021/acs.accounts.0c00488.
[6] J. Zhang, Y. Yuan, L. Gao, G. Zeng, M. Li, H. Huang, Stabilizing Pt-based electrocatalysts for oxygen reduction reaction: fundamental understanding and design strategies, Adv. Mater. 33 (2021) 2006494, https://doi.org/10.1002/adma.202006494.
[7] S. Hussain, H. Erikson, N. Kongi, A. Sarapuu, J. Solla-Gullón, G. Maia, A. M. Kannan, N. Alonso-Vante, K. Tammeveski, Oxygen reduction reaction on nanostructured Pt-based electrocatalysts: a review, Int. J. Hydrog. Energy 45 (2020) 31775–31797, https://doi.org/10.1016/j.ijhydene.2020.08.215.
[8] Z. Ma, Z.P. Cano, A. Yu, Z. Chen, G. Jiang, X. Fu, L. Yang, T. Wu, Z. Bai, J. Lu, Enhancing oxygen reduction activity of pt-based electrocatalysts: from theoretical mechanisms to practical methods, Angew. Chem. Int. Ed. 59 (2020) 18334–18348, https://doi.org/10.1002/anie.202003654.
[9] M. Liu, X. Xiao, Q. Li, L. Luo, M. Ding, B. Zhang, Y. Li, J. Zou, B. Jiang, Recent progress of electrocatalysts for oxygen reduction in fuel cells, J. Colloid Interface Sci. 607 (2022) 791–815, https://doi.org/10.1016/j.jcis.2021.09.008.
[10] A. Kostuch, I.A. Rutkowska, B. Dembinska, A. Wadas, E. Negro, K. Vezzù, V. Di Noto, P.J. Kulesza, Enhancement of activity and development of low Pt content electrocatalysts for oxygen reduction reaction in acid media, Molecules. 26 (2021), https://doi.org/10.3390/molecules26175147.
[11] X. Li, D. Wang, S. Zha, Y. Chu, L. Pan, M. Wu, C. Liu, W. Wang, N. Mitsuzaki, Z. Chen, Active sites identification and engineering of M-N-C electrocatalysts toward oxygen reduction reaction, Int. J. Hydrog. Energy 51 (2024) 1110–1127, https://doi.org/10.1016/j.ijhydene.2023.07.161.
[12] J.R. Varcoe, P. Atanassov, D.R. Dekel, A.M. Herring, M.A. Hickner, Paul.A. Kohl, A.R. Kucernak, W.E. Mustain, K. Nijmeijer, K. Scott, T. Xu, L. Zhuang, Anion-exchange membranes in electrochemical energy systems, Energy Environ. Sci. 7 (2014) 3135–3191, https://doi.org/10.1039/C4EE01303D.
[13] D.R. Dekel, Review of cell performance in anion exchange membrane fuel cells, J. Power Sources 375 (2018) 158–169, https://doi.org/10.1016/j.jpowsour.2017.07.117.
[14] S. Gottesfeld, D.R. Dekel, M. Page, C. Bae, Y. Yan, P. Zelenay, Y.S. Kim, Anion exchange membrane fuel cells: current status and remaining challenges, J. Power Sources 375 (2018) 170–184, https://doi.org/10.1016/j.jpowsour.2017.08.010.
[15] A. Sarapuu, E. Kibena-Põldsepp, M. Borghei, K. Tammeveski, Electrocatalysis of oxygen reduction on heteroatom-doped nanocarbons and transition metal–nitrogen–carbon catalysts for alkaline membrane fuel cells, J. Mater. Chem. A 6 (2018) 776–804, https://doi.org/10.1039/C7TA08690C.
[16] J. Hyun, H.-T. Kim, Powering the hydrogen future: current status and challenges of anion exchange membrane fuel cells, Energy Environ. Sci. 16 (2023) 5633–5662, https://doi.org/10.1039/D3EE01768K.
[17] C. Santoro, P. Bollella, B. Erable, P. Atanassov, D. Pant, Oxygen reduction reaction electrocatalysis in neutral media for bioelectrochemical systems, Nat. Catal. 5 (2022) 473–484, https://doi.org/10.1038/s41929-022-00787-2.
[18] S. Gupta, S. Zhao, O. Ogoke, Y. Lin, H. Xu, G. Wu, Engineering Favorable Morphology and Structure of Fe-N-C Oxygen-Reduction Catalysts through Tuning of Nitrogen/Carbon Precursors, ChemSusChem. 10 (2017) 774–785, https://doi.org/10.1002/cssc.201601397.
[19] D. Sebastián, A. Serov, K. Artyushkova, J. Gordon, P. Atanassov, A.S. Aricò, V. Baglio, High performance and cost-effective direct methanol fuel cells: Fe-N-C methanol-tolerant oxygen reduction reaction catalysts, ChemSusChem. 9 (2016) 1986–1995, https://doi.org/10.1002/cssc.201600583.
[20] Md.M. Hossen, Md.S. Hasan, Md.R.I. Sardar, J. bin Haider, K. Tammeveski Mottakin, P. Atanassov, State-of-the-art and developmental trends in platinum group metal-free cathode catalyst for anion exchange membrane fuel cell (AEMFC), Appl. Catal. B Environ. 325 (2023) 121733, https://doi.org/10.1016/j.apcatb.2022.121733.
[21] X. Huang, T. Shen, T. Zhang, H. Qiu, X. Gu, Z. Ali, Y. Hou, Efficient oxygen reduction catalysts of porous carbon nanostructures decorated with transition metal species, Adv. Energy Mater. 10 (2020) 1900375, https://doi.org/10.1002/aenm.201900375.
[22] G. Wu, A. Santandreu, W. Kellogg, S. Gupta, O. Ogoke, H. Zhang, H.-L. Wang, L. Dai, Carbon nanocomposite catalysts for oxygen reduction and evolution reactions: from nitrogen doping to transition-metal addition, Electrocatalysis 29 (2016) 83–110, https://doi.org/10.1016/j.nanoen.2015.12.032.
[23] G. Wu, P. Zelenay, Nanostructured nonprecious metal catalysts for oxygen reduction reaction, Acc. Chem. Res. 46 (2013) 1878–1889, https://doi.org/10.1021/ar400011z.
[24] L. Osmieri, Transition metal–nitrogen–carbon (M–N–C) catalysts for oxygen reduction reaction. insights on synthesis and performance in polymer electrolyte

fuel cells, ChemEngineering 3 (2019), https://doi.org/10.3390/chemengineering3010016.
[25] A. Sarapuu, J. Lilloja, S. Akula, J.H. Zagal, S. Specchia, K. Tammeveski, Recent advances in non-precious metal single-atom electrocatalysts for oxygen reduction reaction in low-temperature polymer-electrolyte fuel cells, ChemCatChem. 15 (2023) e202300849, https://doi.org/10.1002/cctc.202300849.
[26] X. Xie, H. Peng, G. Ma, Z. Lei, Y. Xu, Recent progress in heteroatom doping to modulate the coordination environment of M–N–C catalysts for the oxygen reduction reaction, Mater. Chem. Front. 7 (2023) 2595–2619, https://doi.org/10.1039/D3QM00096F.
[27] Y. Zhou, Y. Yu, D. Ma, A.C. Foucher, L. Xiong, J. Zhang, E.A. Stach, Q. Yue, Y. Kang, Atomic Fe dispersed hierarchical mesoporous Fe–N–C nanostructures for an efficient oxygen reduction reaction, ACS. Catal. 11 (2021) 74–81, https://doi.org/10.1021/acscatal.0c03496.
[28] L. Peng, J. Yang, Y. Yang, F. Qian, Q. Wang, D. Sun-Waterhouse, L. Shang, T. Zhang, G.I.N. Waterhouse, Mesopore-rich Fe–N–C catalyst with FeN4–O–NC single-atom sites delivers remarkable oxygen reduction reaction performance in alkaline media, Adv. Mater. 34 (2022) 2202544, https://doi.org/10.1002/adma.202202544.
[29] X. Zhang, L. Truong-Phuoc, T. Asset, S. Pronkin, C. Pham-Huu, Are Fe–N–C electrocatalysts an alternative to Pt-based electrocatalysts for the next generation of proton exchange membrane fuel cells? ACS. Catal. 12 (2022) 13853–13875, https://doi.org/10.1021/acscatal.2c02146.
[30] K. Artyushkova, A. Serov, S. Rojas-Carbonell, P. Atanassov, Chemistry of multitudinous active sites for oxygen reduction reaction in transition metal–nitrogen–carbon electrocatalysts, J. Phys. Chem. C 119 (2015) 25917–25928, https://doi.org/10.1021/acs.jpcc.5b07653.
[31] H. Shen, T. Thomas, S.A. Rasaki, A. Saad, C. Hu, J. Wang, M. Yang, Oxygen reduction reactions of Fe-N-C catalysts: current status and the way forward, Electrochem. Energy Rev. 2 (2019) 252–276, https://doi.org/10.1007/s41918-019-00030-w.
[32] T. Marshall-Roth, N.J. Libretto, A.T. Wrobel, K.J. Anderton, M.L. Pegis, N. D. Ricke, T.V. Voorhis, J.T. Miller, Y. Surendranath, A pyridinic Fe-N4 macrocycle models the active sites in Fe/N-doped carbon electrocatalysts, Nat. Commun. 11 (2020) 5283, https://doi.org/10.1038/s41467-020-18969-6.
[33] O.P. Gurjar, P. Saini, S. Kumari, K. Atal, U. Phageria, S. Bugalia, A review on recent advances of iron-based macrocyclic complexes as prominent candidate for several potential applications, J. Iran. Chem. Soc. 21 (2024) 305–326, https://doi.org/10.1007/s13738-023-02934-3.
[34] H. Wang, D.-J. Liu, Rational design of platinum-group-metal-free electrocatalysts for oxygen reduction reaction, Curr. Opin. Electrochem. 28 (2021) 100724, https://doi.org/10.1016/j.coelec.2021.100724.
[35] J. Cui, Q. Chen, X. Li, S. Zhang, Recent advances in non-precious metal electrocatalysts for oxygen reduction in acidic media and PEMFCs: an activity, stability and mechanism study, Green. Chem. 23 (2021) 6898–6925, https://doi.org/10.1039/D1GC01040A.
[36] F. Luo, S. Wagner, I. Onishi, S. Selve, S. Li, W. Ju, H. Wang, J. Steinberg, A. Thomas, U.I. Kramm, P. Strasser, Surface site density and utilization of platinum group metal (PGM)-free Fe–NC and FeNi–NC electrocatalysts for the oxygen reduction reaction, Chem. Sci. 12 (2021) 384–396, https://doi.org/10.1039/D0SC03280H.
[37] S.A. Mirshokraee, M. Muhyuddin, J. Orsilli, E. Berretti, L. Capozzoli, A. Lavacchi, C. Lo Vecchio, V. Baglio, A. Galli, A. Zaffora, F. Di Franco, M. Santamaria, L. Olivi, S. Pollastri, C. Santoro, Mono-, bi- and tri-metallic platinum group metal-free electrocatalysts for hydrogen evolution reaction following a facile synthetic route, Ind. Chem. Mater. 1 (2023) 343–359, https://doi.org/10.1039/D3IM00058C.
[38] G. Zuccante, M. Acciarri, C.L. Vecchio, I. Gatto, V. Baglio, N. Pianta, R. Ruffo, L. Navarini, C. Santoro, Oxygen reduction reaction platinum group metal-free electrocatalysts derived from spent coffee grounds, Electrochim. Acta 492 (2024) 144353, https://doi.org/10.1016/j.electacta.2024.144353.
[39] M. Muhyuddin, A. Friedman, F. Poli, E. Petri, H. Honig, F. Basile, A. Fasolini, R. Lorenzi, E. Berretti, M. Bellini, A. Lavacchi, L. Elbaz, C. Santoro, F. Soavi, Lignin-derived bimetallic platinum group metal-free oxygen reduction reaction electrocatalysts for acid and alkaline fuel cells, J. Power Sources 556 (2023) 232416, https://doi.org/10.1016/j.jpowsour.2022.232416.
[40] S. Akula, M. Mooste, J. Kozlova, M. Käärik, A. Treshchalov, A. Kikas, V. Kisand, J. Aruväli, P. Paiste, A. Tamm, J. Leis, K. Tammeveski, Transition metal (Fe, Co, Mn, Cu) containing nitrogen-doped porous carbon as efficient oxygen reduction electrocatalysts for anion exchange membrane fuel cells, Chem. Eng. J. 458 (2023) 141468, https://doi.org/10.1016/j.cej.2023.141468.
[41] Y. Kumar, E. Kibena-Põldsepp, M. Mooste, J. Kozlova, A. Kikas, J. Aruväli, M. Käärik, V. Kisand, J. Leis, A. Tamm, S. Holdcroft, J.H. Zagal, K. Tammeveski, Iron and nickel phthalocyanine-modified nanocarbon materials as cathode catalysts for anion-exchange membrane fuel cells and zinc-air batteries**, ChemElectroChem. 9 (2022) e202200717, https://doi.org/10.1002/celc.202200717.
[42] Y. Li, N. Wang, H. Lei, X. Li, H. Zheng, H. Wang, W. Zhang, R. Cao, Bioinspired N4-metallomacrocycles for electrocatalytic oxygen reduction reaction, Coord. Chem. Rev. 442 (2021) 213996, https://doi.org/10.1016/j.ccr.2021.213996.
[43] C. Di Natale, C.P. Gros, R. Paolesse, Corroles at work: a small macrocycle for great applications, Chem. Soc. Rev. 51 (2022) 1277–1335, https://doi.org/10.1039/D1CS00662B.
[44] J.An Jyoti, D. Kim, D.G. Churchill, A. Kumar, Cobalt corroles: synthesis and applications, Coord. Chem. Rev. 511 (2024) 215869, https://doi.org/10.1016/j.ccr.2024.215869.
[45] X. Li, H. Lei, L. Xie, N. Wang, W. Zhang, R. Cao, Metalloporphyrins as catalytic models for studying hydrogen and oxygen evolution and oxygen reduction reactions, Acc. Chem. Res. 55 (2022) 878–892, https://doi.org/10.1021/acs.accounts.1c00753.
[46] N. Levy, L. Elbaz, Design of PGM -free ORR catalysts: from molecular to the state of the art, Electrocatal. Membr. Fuel Cells (2023) 175–203, https://doi.org/10.1002/9783527830572.ch6.
[47] A. Kumar, Y. Zhang, W. Liu, X. Sun, The chemistry, recent advancements and activity descriptors for macrocycles based electrocatalysts in oxygen reduction reaction, Coord. Chem. Rev. 402 (2020) 213047, https://doi.org/10.1016/j.ccr.2019.213047.
[48] H. Maeda, K. Takada, N. Fukui, S. Nagashima, H. Nishihara, Conductive coordination nanosheets: sailing to electronics, energy storage, and catalysis, Coord. Chem. Rev. 470 (2022) 214693, https://doi.org/10.1016/j.ccr.2022.214693.
[49] M. Muhyuddin, E. Berretti, S.A. Mirshokraee, J. Orsilli, R. Lorenzi, L. Capozzoli, F. D'Acapito, E. Murphy, S. Guo, P. Atanassov, A. Lavacchi, C. Santoro, Formation of the active site structures during pyrolysis transformation of Fe-phthalocyanine into Fe-Nx-C electrocatalysts for the oxygen reduction reaction, Appl. Catal. B Environ. 343 (2024) 123515, https://doi.org/10.1016/j.apcatb.2023.123515.
[50] S. Chen, M. Cui, Z. Yin, J. Xiong, L. Mi, Y. Li, Single-atom and dual-atom electrocatalysts derived from metal organic frameworks: current progress and perspectives, ChemSusChem. 14 (2021) 73–93, https://doi.org/10.1002/cssc.202002098.
[51] C. Li, H. Zhang, M. Liu, F.-F. Lang, J. Pang, X.-H. Bu, Recent progress in metal–organic frameworks (MOFs) for electrocatalysis, Ind, Chem. Mater. 1 (2023) 9–38, https://doi.org/10.1039/D2IM00063F.
[52] W. Zhao, G. Wan, C. Peng, H. Sheng, J. Wen, H. Chen, Key Single-Atom Electrocatalysis in Metal—Organic Framework (MOF)-Derived Bifunctional Catalysts, ChemSusChem. 11 (2018) 3473–3479, https://doi.org/10.1002/cssc.201801473.
[53] Y. Luo, J. Zhang, M. Kiani, Y. Chen, J. Chen, G. Wang, S.H. Chan, R. Wang, Synthesis of MOF-Derived Nonprecious Catalyst with High Electrocatalytic Activity for Oxygen Reduction Reaction, Ind. Eng. Chem. Res. 57 (2018) 12087–12095, https://doi.org/10.1021/acs.iecr.8b02744.
[54] J.-N. Liu, B.-Q. Li, C.-X. Zhao, J. Yu, Q. Zhang, A composite bifunctional oxygen electrocatalyst for high-performance rechargeable zinc–air batteries, ChemSusChem. 13 (2020) 1529–1536, https://doi.org/10.1002/cssc.201903071.
[55] A. Zitolo, V. Goellner, V. Armel, M.-T. Sougrati, T. Mineva, L. Stievano, E. Fonda, F. Jaouen, Identification of catalytic sites for oxygen reduction in iron- and nitrogen-doped graphene materials, Nat. Mater. 14 (2015) 937–942, https://doi.org/10.1038/nmat4367.
[56] E. Proietti, F. Jaouen, M. Lefèvre, N. Larouche, J. Tian, J. Herranz, J.-P. Dodelet, Iron-based cathode catalyst with enhanced power density in polymer electrolyte membrane fuel cells, Nat. Commun. 2 (2011) 416, https://doi.org/10.1038/ncomms1427.
[57] A. Morozan, F. Jaouen, Metal organic frameworks for electrochemical applications, Energy Environ. Sci. 5 (2012) 9269–9290, https://doi.org/10.1039/C2EE22989G.
[58] A. Friedman, L. Landau, S. Gonen, Z. Gross, L. Elbaz, Efficient bio-inspired oxygen reduction electrocatalysis with electropolymerized cobalt corroles, ACS. Catal. 8 (2018) 5024–5031, https://doi.org/10.1021/acscatal.8b00876.
[59] L. Peles-Strahl, N. Zion, O. Lori, N. Levy, G. Bar, A. Dahan, L. Elbaz, Bipyridine modified conjugated carbon aerogels as a platform for the electrocatalysis of oxygen reduction reaction, Adv. Funct. Mater. 31 (2021) 2100163, https://doi.org/10.1002/adfm.202100163.
[60] A.D. Adler, F.R. Longo, J.D. Finarelli, J. Goldmacher, J. Assour, L. Korsakoff, A simplified synthesis for meso-tetraphenylporphine, J. Org. Chem. 32 (1967) 476, https://doi.org/10.1021/jo01288a053. –476.
[61] A. Serov, M.H. Robson, M. Smolnik, P. Atanassov, Templated bi-metallic non-PGM catalysts for oxygen reduction, Electrochim. Acta 80 (2012) 213–218, https://doi.org/10.1016/j.electacta.2012.07.008.
[62] M. Muhyuddin, D. Testa, R. Lorenzi, G.M. Vanacore, F. Poli, F. Soavi, S. Specchia, W. Giurlani, M. Innocenti, L. Rosi, C. Santoro, Iron-based electrocatalysts derived from scrap tires for oxygen reduction reaction: evolution of synthesis-structure-performance relationship in acidic, neutral and alkaline media, Electrochim. Acta 433 (2022) 141254, https://doi.org/10.1016/j.electacta.2022.141254.
[63] S. Zago, M. Bartoli, M. Muhyuddin, G.M. Vanacore, P. Jagdale, A. Tagliaferro, C. Santoro, S. Specchia, Engineered biochar derived from pyrolyzed waste tea as a carbon support for Fe-N-C electrocatalysts for the oxygen reduction reaction, Electrochim. Acta 412 (2022) 140128, https://doi.org/10.1016/j.electacta.2022.140128.
[64] D. Testa, G. Zuccante, M. Muhyuddin, R. Landone, A. Scommegna, R. Lorenzi, M. Acciarri, E. Petri, F. Soavi, L. Poggini, L. Capozzoli, A. Lavacchi, N. Lamanna, A. Franzetti, L. Zoia, C. Santoro, Giving new life to waste cigarette butts: transformation into platinum group metal-free electrocatalysts for oxygen reduction reaction in acid, neutral and alkaline environment, Catalysts. 13 (2023), https://doi.org/10.3390/catal13030635.
[65] C.Lo Vecchio, A.S. Aricò, V. Baglio, Application of low-Cost Me-N-C (Me = Fe or Co) electrocatalysts derived from EDTA in direct methanol fuel cells (DMFCs), Materials. (Basel) 11 (2018), https://doi.org/10.3390/ma11071193.
[66] R. Gokhale, Y. Chen, A. Serov, K. Artyushkova, P. Atanassov, Direct synthesis of platinum group metal-free Fe-N-C catalyst for oxygen reduction reaction in alkaline media, Electrochem. Commun. 72 (2016) 140–143, https://doi.org/10.1016/j.elecom.2016.09.013.

[67] S.A. Mirshokraee, M. Muhyuddin, R. Lorenzi, G. Tseberlidis, C.L. Vecchio, V. Baglio, E. Berretti, A. Lavacchi, C. Santoro, Litchi-derived platinum group metal-free electrocatalysts for oxygen reduction reaction and hydrogen evolution reaction in alkaline media, SusMat 3 (2023) 248–262, https://doi.org/10.1002/sus2.121.
[68] R. Mercado, C. Wahl, J.En Lu, T. Zhang, B. Lu, P. Zhang, J.Q. Lu, A. Allen, J. Z. Zhang, S. Chen, Nitrogen-doped porous carbon cages for electrocatalytic reduction of oxygen: enhanced performance with iron and cobalt dual metal centers, ChemCatChem. 12 (2020) 3230–3239, https://doi.org/10.1002/cctc.201902324.
[69] A. Serov, K. Artyushkova, N.I. Andersen, S. Stariha, P. Atanassov, Original mechanochemical synthesis of non-platinum group metals oxygen reduction reaction catalysts assisted by sacrificial support method, ubiquitus electrochem. 179 (2015) 154–160. https://doi.org/10.1016/j.electacta.2015.02.108.
[70] K. Singh, F. Razmjooei, J.-S. Yu, Active sites and factors influencing them for efficient oxygen reduction reaction in metal-N coordinated pyrolyzed and non-pyrolyzed catalysts: a review, J. Mater. Chem. A 5 (2017) 20095–20119, https://doi.org/10.1039/C7TA05222G.
[71] C.Z. Loyola, S. Ureta-Zañartu, J.H. Zagal, F. Tasca, Activity volcano plots for the oxygen reduction reaction using FeN4 complexes: from reported experimental data to the electrochemical meaning, Curr. Opin. Electrochem. 32 (2022) 100923, https://doi.org/10.1016/j.coelec.2021.100923.
[72] R. Cao, R. Thapa, H. Kim, X. Xu, M. Gyu Kim, Q. Li, N. Park, M. Liu, J. Cho, Promotion of oxygen reduction by a bio-inspired tethered iron phthalocyanine carbon nanotube-based catalyst, Nat. Commun. 4 (2013) 2076, https://doi.org/10.1038/ncomms3076.
[73] Z. Zhang, M. Dou, J. Ji, F. Wang, Phthalocyanine tethered iron phthalocyanine on graphitized carbon black as superior electrocatalyst for oxygen reduction reaction, Nano Energy 34 (2017) 338–343, https://doi.org/10.1016/j.nanoen.2017.02.042.
[74] S. Yamazaki, Metalloporphyrins and related metallomacrocycles as electrocatalysts for use in polymer electrolyte fuel cells and water electrolyzers, Coord. Chem. Energy 373 (2018) 148–166, https://doi.org/10.1016/j.ccr.2017.09.016.
[75] R. Praats, M. Käärik, A. Kikas, V. Kisand, J. Aruväli, P. Paiste, M. Merisalu, J. Leis, V. Sammelselg, J.H. Zagal, S. Holdcroft, N. Nakashima, K. Tammeveski, Electrocatalytic oxygen reduction reaction on iron phthalocyanine-modified carbide-derived carbon/carbon nanotube composite electrocatalysts, Electrochim. Acta 334 (2020) 135575, https://doi.org/10.1016/j.electacta.2019.135575.
[76] R. Praats, I. Kruusenberg, M. Käärik, U. Joost, J. Aruväli, P. Paiste, R. Saar, P. Rauwel, M. Kook, J. Leis, J.H. Zagal, K. Tammeveski, Electroreduction of oxygen in alkaline solution on iron phthalocyanine modified carbide-derived carbons, Electrochim. Acta 299 (2019) 999–1010, https://doi.org/10.1016/j.electacta.2019.01.062.
[77] Iron(II) phthalocyanine (€/g), Sigma-Aldrich (n.d.). https://www.sigmaaldrich.com/IT/it/search/iron-phtalocyanine?focus=products&page=1&perpage=30&sort=relevance&term=iron%20phtalocyanine&type=product.
[78] M. Sevilla, A.B. Fuertes, Catalytic graphitization of templated mesoporous carbons, Carbon. N. Y. 44 (2006) 468–474, https://doi.org/10.1016/j.carbon.2005.08.019.
[79] M. Inagaki, New Carbons - Control of Structure and Functions, Elsevier Science, 2000. https://books.google.it/books?id=IdelPW03XI4C.
[80] H. Peng, Z. Mo, S. Liao, H. Liang, L. Yang, F. Luo, H. Song, Y. Zhong, B. Zhang, High Performance Fe- and N- Doped Carbon Catalyst with Graphene Structure for Oxygen Reduction, Sci. Rep. 3 (2013) 1765, https://doi.org/10.1038/srep01765.
[81] A.C. Ferrari, J. Robertson, Interpretation of Raman spectra of disordered and amorphous carbon, Phys. Rev. B 61 (2000) 14095–14107, https://doi.org/10.1103/PhysRevB.61.14095.
[82] L.G. Cançado, A. Jorio, E.H.M. Ferreira, F. Stavale, C.A. Achete, R.B. Capaz, M.V. O. Moutinho, A. Lombardo, T.S. Kulmala, A.C. Ferrari, Quantifying defects in graphene via Raman spectroscopy at different excitation energies, Nano Lett. 11 (2011) 3190–3196, https://doi.org/10.1021/nl201432g.
[83] L.M. Malard, M.A. Pimenta, G. Dresselhaus, M.S. Dresselhaus, Raman spectroscopy in graphene, Phys. Rep. 473 (2009) 51–87, https://doi.org/10.1016/j.physrep.2009.02.003.
[84] C. Zhu, Q. Shi, B.Z. Xu, S. Fu, G. Wan, C. Yang, S. Yao, J. Song, H. Zhou, D. Du, S. P. Beckman, D. Su, Y. Lin, Hierarchically porous M–N–C (M = Co and Fe) single-atom electrocatalysts with robust MNx active moieties enable enhanced ORR performance, Adv. Energy Mater. 8 (2018) 1801956, https://doi.org/10.1002/aenm.201801956.
[85] F. Jaouen, J.-P. Dodelet, O2 reduction mechanism on non-noble metal catalysts for PEM fuel cells. Part I: experimental rates of O2 electroreduction, H2O2 electroreduction, and H2O2 disproportionation, J. Phys. Chem. C 113 (2009) 15422–15432, https://doi.org/10.1021/jp900837e.
[86] A. Serov, U. Tylus, K. Artyushkova, S. Mukerjee, P. Atanassov, Mechanistic studies of oxygen reduction on Fe-PEI derived non-PGM electrocatalysts, Appl. Catal. B Environ 150–151 (2014) 179–186, https://doi.org/10.1016/j.apcatb.2013.12.009.
[87] L. Osmieri, C. Zafferoni, L. Wang, A.H.A. Monteverde Videla, A. Lavacchi, S. Specchia, Polypyrrole-derived Fe−Co−N−C catalyst for the oxygen reduction reaction: performance in alkaline hydrogen and ethanol fuel cells, ChemElectroChem. 5 (2018) 1954–1965, https://doi.org/10.1002/celc.201800420.
[88] M. Primbs, Y. Sun, A. Roy, D. Malko, A. Mehmood, M.-T. Sougrati, P.-Y. Blanchard, G. Granozzi, T. Kosmala, G. Daniel, P. Atanassov, J. Sharman, C. Durante, A. Kucernak, D. Jones, F. Jaouen, P. Strasser, Establishing reactivity descriptors for platinum group metal (PGM)-free Fe–N–C catalysts for PEM fuel cells, Energy Environ. Sci. 13 (2020) 2480–2500, https://doi.org/10.1039/D0EE01013H.
[89] K. Artyushkova, S. Rojas-Carbonell, C. Santoro, E. Weiler, A. Serov, R. Awais, R. R. Gokhale, P. Atanassov, Correlations between synthesis and performance of fe-based pgm-free catalysts in acidic and alkaline media: evolution of surface chemistry and morphology, ACS Appl. Energy Mater. 2 (2019) 5406–5418, https://doi.org/10.1021/acsaem.9b00331.
[90] K. Artyushkova, Misconceptions in interpretation of nitrogen chemistry from x-ray photoelectron spectra, J. Vac. Sci. Technol. A 38 (2020) 031002, https://doi.org/10.1116/1.5135923.
[91] G. Yang, J. Zhu, P. Yuan, Y. Hu, G. Qu, B.-A. Lu, X. Xue, H. Yin, W. Cheng, J. Cheng, W. Xu, J. Li, J. Hu, S. Mu, J.-N. Zhang, Regulating Fe-spin state by atomically dispersed Mn-N in Fe-N-C catalysts with high oxygen reduction activity, Nat. Commun. 12 (2021) 1734, https://doi.org/10.1038/s41467-021-21919-5.
[92] Y. Pan, M. Li, W. Mi, M. Wang, J. Li, Y. Zhao, X. Ma, B. Wang, W. Zhu, Z. Cui, H. Yin, Y. Liu, Single-atomic Mn sites coupled with Fe3C nanoparticles encapsulated in carbon matrixes derived from bimetallic Mn/Fe polyphthalocyanine conjugated polymer networks for accelerating electrocatalytic oxygen reduction, Nano Res. 15 (2022) 7976–7985, https://doi.org/10.1007/s12274-022-4502-4.
[93] A. Kozhushner, N. Zion, L. Elbaz, Methods for assessment and measurement of the active site density in platinum group metal–free oxygen reduction reaction catalysts, Curr. Opin. Electrochem. 25 (2021) 100620, https://doi.org/10.1016/j.coelec.2020.08.002.
[94] E. Luo, Y. Chu, J. Liu, Z. Shi, S. Zhu, L. Gong, J. Ge, C.H. Choi, C. Liu, W. Xing, Pyrolyzed M–Nx catalysts for oxygen reduction reaction: progress and prospects, Energy Environ. Sci. 14 (2021) 2158–2185, https://doi.org/10.1039/D1EE00142F.
[95] M.-X. Chen, L. Tong, H.-W. Liang, Understanding the Catalytic Sites of Metal–Nitrogen–Carbon Oxygen Reduction Electrocatalysts, Chem. – Eur. J 27 (2021) 145–157, https://doi.org/10.1002/chem.202002427.
[96] Y. He, S. Liu, C. Priest, Q. Shi, G. Wu, Atomically dispersed metal–nitrogen–carbon catalysts for fuel cells: advances in catalyst design, electrode performance, and durability improvement, Chem. Soc. Rev. 49 (2020) 3484–3524, https://doi.org/10.1039/C9CS00903E.
[97] T. Asset, P. Atanassov, Iron-nitrogen-carbon catalysts for proton exchange membrane fuel cells, Joule 4 (2020) 33–44, https://doi.org/10.1016/j.joule.2019.12.002.
[98] Y. Chen, I. Matanovic, E. Weiler, P. Atanassov, K. Artyushkova, Mechanism of oxygen reduction reaction on transition metal–nitrogen–carbon catalysts: establishing the role of nitrogen-containing active sites, ACS Appl. Energy Mater. 1 (2018) 5948–5953, https://doi.org/10.1021/acsaem.8b00959.
[99] Á. García, T. Haynes, M. Retuerto, P. Ferrer, L. Pascual, M.A. Peña, M. Abdel Salam, M. Mokhtar, D. Gianolio, S. Rojas, Effect of the thermal treatment of Fe/N/C catalysts for the oxygen reduction reaction synthesized by pyrolysis of covalent organic frameworks, Ind. Eng. Chem. Res. 60 (2021) 18759–18769, https://doi.org/10.1021/acs.iecr.1c02841.
[100] C. Santoro, A. Serov, R. Gokhale, S. Rojas-Carbonell, L. Stariha, J. Gordon, K. Artyushkova, P. Atanassov, A family of Fe-N-C oxygen reduction electrocatalysts for microbial fuel cell (MFC) application: relationships between surface chemistry and performances, Appl. Catal. B Environ. 205 (2017) 24–33, https://doi.org/10.1016/j.apcatb.2016.12.013.
[101] S. Kabir, K. Artyushkova, A. Serov, P. Atanassov, Role of nitrogen moieties in N-doped 3D-graphene nanosheets for oxygen electroreduction in acidic and alkaline media, ACS Appl. Mater. Interfaces 10 (2018) 11623–11632, https://doi.org/10.1021/acsami.7b18651.
[102] J.H. Zagal, Metallophthalocyanines as catalysts in electrochemical reactions, Coord. Chem. Rev. 119 (1992) 89–136, https://doi.org/10.1016/0010-8545(92)80031-L.
[103] Y. Han, Y. Wang, R. Xu, W. Chen, L. Zheng, A. Han, Y. Zhu, J. Zhang, H. Zhang, J. Luo, C. Chen, Q. Peng, D. Wang, Y. Li, Electronic structure engineering to boost oxygen reduction activity by controlling the coordination of the central metal, Energy Environ. Sci. 11 (2018) 2348–2352, https://doi.org/10.1039/C8EE01481G.
[104] K. Chen, K. Liu, P. An, H. Li, Y. Lin, J. Hu, C. Jia, J. Fu, H. Li, H. Liu, Z. Lin, W. Li, J. Li, Y.-R. Lu, T.-S. Chan, N. Zhang, M. Liu, Iron phthalocyanine with coordination induced electronic localization to boost oxygen reduction reaction, Nat. Commun. 11 (2020) 4173, https://doi.org/10.1038/s41467-020-18062-y.
[105] H. Jia, Z. Sun, D. Jiang, S. Yang, P. Du, An iron porphyrin-based conjugated network wrapped around carbon nanotubes as a noble-metal-free electrocatalyst for efficient oxygen reduction reaction, Inorg. Chem. Front. 3 (2016) 821–827, https://doi.org/10.1039/C5QI00198F.
[106] T.P. Dung, V. Chihaia, D.N. Son, Effects of functional groups in iron porphyrin on the mechanism and activity of oxygen reduction reaction, RSC. Adv. 13 (2023) 8523–8534, https://doi.org/10.1039/D2RA08007A.
[107] Z. Liang, H.-Y. Wang, H. Zheng, W. Zhang, R. Cao, Porphyrin-based frameworks for oxygen electrocatalysis and catalytic reduction of carbon dioxide, Chem. Soc. Rev. 50 (2021) 2540–2581, https://doi.org/10.1039/D0CS01482F.
[108] Y. Cao, Y. Mou, J. Zhang, R. Zhang, Z. Liang, Porphyrin-based frameworks and derivatives for the oxygen reduction reaction, Mater. Today Catal 4 (2024) 100044, https://doi.org/10.1016/j.mtcata.2024.100044.
[109] V.S. Bagotzky, M.R. Tarasevich, K.A. Radyushkina, O.A. Levina, S.I. Andrusyova, Electrocatalysis of the oxygen reduction process on metal chelates in acid

electrolyte, J. Power Sources 2 (1978) 233–240, https://doi.org/10.1016/0378-7753(78)85014-9.
[110] J.A.R. van Veen, H.A. Colijn, J.F. van Baar, On the effect of a heat treatment on the structure of carbon-supported metalloporphyrins and phthalocyanines, Electrochim. Acta 33 (1988) 801–804, https://doi.org/10.1016/S0013-4686(98)80010-8.
[111] F. Vallejos-Burgos, S. Utsumi, Y. Hattori, X. García, A.L. Gordon, H. Kanoh, K. Kaneko, L.R. Radovic, Pyrolyzed phthalocyanines as surrogate carbon catalysts: initial insights into oxygen-transfer mechanisms, Fuel 99 (2012) 106–117, https://doi.org/10.1016/j.fuel.2012.03.055.
[112] M. Muhyuddin, P. Mustarelli, C. Santoro, Recent advances in waste plastic transformation into valuable platinum-group metal-free electrocatalysts for oxygen reduction reaction, ChemSusChem. 14 (2021) 3785–3800, https://doi.org/10.1002/cssc.202101252.
[113] M. Borghei, J. Lehtonen, L. Liu, O.J. Rojas, Advanced biomass-derived electrocatalysts for the oxygen reduction reaction, Adv. Mater. 30 (2018) 1703691, https://doi.org/10.1002/adma.201703691.
[114] G. Zuccante, M. Muhyuddin, V.C.A. Ficca, E. Placidi, M. Acciarri, N. Lamanna, A. Franzetti, L. Zoia, M. Bellini, E. Berretti, A. Lavacchi, C. Santoro, Transforming cigarette wastes into oxygen reduction reaction electrocatalyst: does each component behave differently? An experimental evaluation, ChemElectroChem. 11 (2024) e202300725, https://doi.org/10.1002/celc.202300725.
[115] M. Muhyuddin, J. Filippi, L. Zoia, S. Bonizzoni, R. Lorenzi, E. Berretti, L. Capozzoli, M. Bellini, C. Ferrara, A. Lavacchi, C. Santoro, Waste face surgical mask transformation into crude oil and nanostructured electrocatalysts for fuel cells and electrolyzers, ChemSusChem. 15 (2022) e202102351, https://doi.org/10.1002/cssc.202102351.
[116] L. Du, G. Zhang, X. Liu, A. Hassanpour, M. Dubois, A.C. Tavares, S. Sun, Biomass-derived nonprecious metal catalysts for oxygen reduction reaction: the demand-oriented engineering of active sites and structures, Carbon Energy 2 (2020) 561–581, https://doi.org/10.1002/cey2.73.